Supplementary Information for

Doubly Crossed Supercoils Built by Cooperative Anion and Metal Coordination

Wei Zhao,[a#*] Hongfei Li,[b#] Xinyu Lian,[a#] Cheng Jin,[a] Di Meng,[b] Boyang Li,[c] Xiaoyan Zheng,[a*] Xiao-Juan Yang[a] and Biao Wu[a*]

[a] Key Laboratory of Medicinal Molecule Science and Pharmaceutics Engineering, Ministry of Industry and Information Technology, School of Chemistry and Chemical Engineering, Beijing Institute of Technology, Beijing 102488, China.

[b] Key Laboratory of Synthetic and Natural Functional Molecule Chemistry of the Ministry of Education, College of Chemistry and Materials Science, Northwest University, Xi'an 710069, China.

[c] College of Chemistry & Pharmacy, Northwest A&F University, Yangling 712100, China.

# These authors contributed equally: Wei Zhao, Hongfei Li, Xinyu Lian.

E-mail: zhaochem@bit.edu.cn; xiaoyanzheng@bit.edu.cn; wubiao@bit.edu.cn

Table of contents:

S1. General Methods

All the reagents were obtained from commercial suppliers and used as received unless otherwise indicated. The solvents and other reagents were of reagent grade and purchased commercially. ^{1}H NMR spectra were recorded on Bruker AVANCE III-400 MHz spectrometers. ^{1}H NMR chemical shifts were reported based on residue solvent peaks (2.50 *ppm* for DMSO-d_6). (*Organometallics* **2010**, *29*, 2176–2179) The mass spectra of ligands and complexes were measured on a Bruker microTOF-Q II ESI-Q-TOF LC/MS/MS spectrometer. Circular Dichroism (CD) spectra and corresponding ultraviolet absorption spectra were recorded on a J-1500 spectropolarimeter (Jasco, Japan). X-ray diffractions were recorded on a Bruker D8 Venture Photon II diffractometer.

S2. Synthetic Procedures of Oligourea Ligands

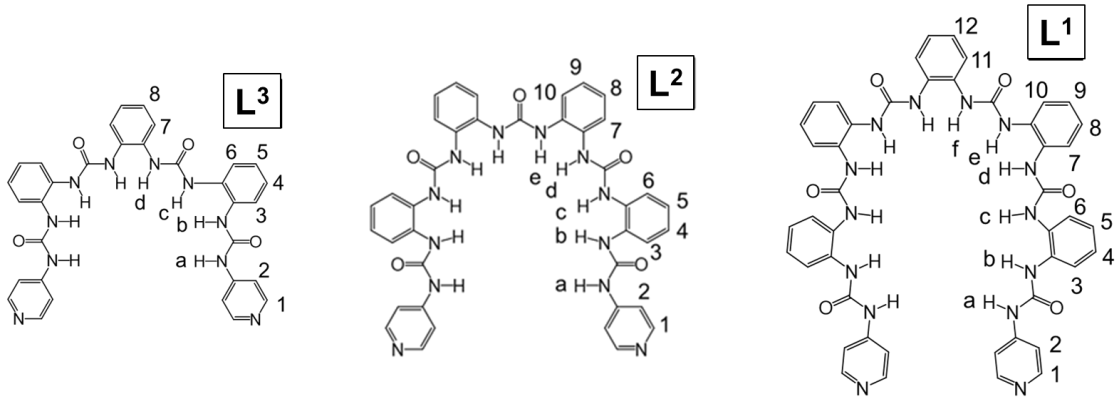

Scheme S1. Chemical structures of pyridyl-oligourea ligands **L^1**, **L^2** and **L^3**.

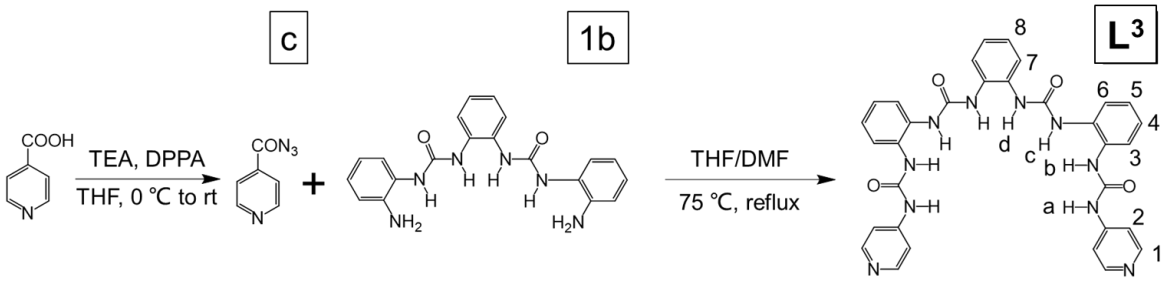

Scheme S2. Synthetic route of preparing ligand **L^3**. Compound **1b** was synthesized according to previously reported procedure (*Org. Lett.* **2012**, *14*, 684–687).

L[3]: Isonicotinic acid (0.5 g, 20 mmol) was added to tetrahydrofuran (20 mL), triethylamine (0.6 mL, 4.3 mmol) was added. After that, all the starting materials were dissolved. DPPA (0.9 mL, 4.1mmol) was added slowly into solution at 0ºC (ice bath). After stirring for 1 h at room temperature, the solvents were removed, and the product was extracted with diethyl ether. The obtained product C (0.50 g, 3.38 mmol) was dissolved in tetrahydrofuran (30 mL) solution, and the solution was stirred at 50 ° C for 20 min. Then, 1b (0.3 g, 0.78 mmol, in DMF, 5 mL) was added dropwise to the above solution. After stringing 12 h, the resulting precipitate was filtered off and washed with ethanol and diethyl ether. The product was dried under vacuum to yield **L[3]** as a white solid. 351 mg, overall yield: 85%. ^{1}H NMR (400 MHz, DMSO-d_6, ppm): δ 9.54 (s, 1H, NHa), 8.51 (s, 1H, NHb), 8.46 (s, 1H, NHc), 8.33 (d, J = 4.0 Hz, 2H, H1), 8.24 (s, 1H, NHd), 7.58−7.53 (m, 3H, H3, H6, H7), 7.41−7.40 (d, J = 4.0 Hz, 2H, H2), 7.10−7.06 (m, 3H, H4, H5, H8). ^{13}C NMR (100 MHz, DMSO-d_6, ppm): δ 154.1 (CO), 152.8 (CO), 150.1 (C), 146.6 (C), 131.4 (C), 131.3 (C), 130.8 (C), 124.5 (CH), 124.3 (CH), 124.2 (CH), 124.2 (CH), 124.1 (CH), 112.2 (CH). ESI-MS: m/z, 100%, 639.2573 $[M+Na]^+$.

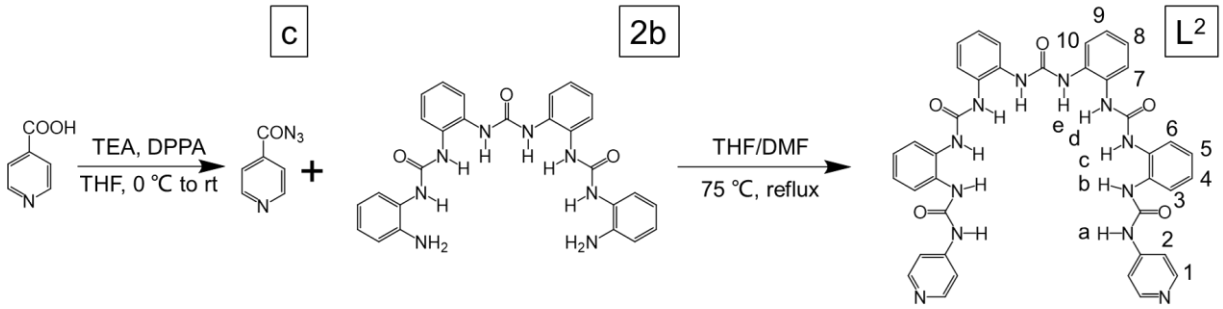

Scheme S3. Synthetic route of preparing ligand **L[2]**. Compound **2b** was synthesized according to previously reported procedure (*Org. Lett.* **2010**, *12*, 5612–5615).

L[2]: The obtained product C (0.50 g, 3.38 mmol) was dissolved in tetrahydrofuran (30 mL) solution, and the solution was stirred at 50 ° C for 20 min. 2b (0.4 g, 0.78 mmol, in DMF, 5 mL) was dropwise added to the solution. After stringing 12 h at the same temperature, the resulting precipitate was filtered and washed with ethanol and diethyl ether. Then, the product was dried under vacuum to yield **L[2]** as a white solid. 353 mg, yield: 70%. ^{1}H NMR (400 MHz, DMSO-d_6, ppm): δ 9.58 (s, 1H, NHa), 8.53 (s, 2H, NHb, NHc), 8.48 (s, 1H, NHd), 8.32 (d, J = 5.6 Hz, 2H, H1), 8.27 (s, 1H, NHe), 7.55 (m, 4H, H3, H6, H7, H10), 7.41 (d, J = 5.6 Hz, 2H, H2), 7.08 (m, 4H, H4, H5, H8, H9). ^{13}C NMR (100 MHz, DMSO-d_6, ppm): δ 154.14 (CO), 152.84 (CO), 150.15

(CO), 146.71 (C), 131.54 (C), 131.34 (C), 131.27 (C), 130.77 (C), 124.57 (CH), 124.31 (CH), 124.25 (CH), 124.19 (CH), 124.14 (CH), 112.26 (CH). ESI-MS: m/z, 100%, 773.3086 $[M+Na]^+$ (calcd. for 773.2667); 26%, 751.3143 $[M+H]^+$ (calcd. for 751.2847).

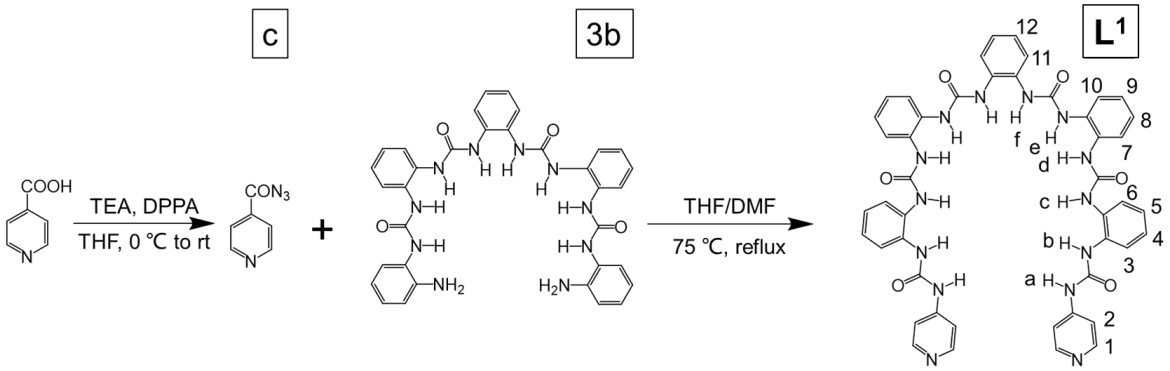

Scheme S3. Synthetic route of preparing ligand $\mathbf{L^1}$. Compound **3b** was synthesized according to previously reported procedures (*Org. Lett.* **2012**, *14*, 684–687).

$\mathbf{L^1}$: The obtained product C (0.50 g, 3.38 mmol) was dissolved in tetrahydrofuran (30 mL) solution, and the solution was stirred at 50 ° C for 20 min. A solution of 3b (0.5 g, 0.78 mmol) in DMF (5 mL) was dropwise added to the reaction solution. After stringing 12 h at the same temperature, the resulting precipitate was filtered off and washed several times with ethanol and diethyl ether. The product was dried under vacuum to yield $\mathbf{L^2}$ as a white solid. 380 mg, yield: 64%. ^{1}H NMR (400 MHz, DMSO-d_6, ppm): δ 9.54 (s, 1H, Ha), 8.50 (s, 3H, Hb, Hc, Hd), 8.45 (s, 1H, He), 8.33 (d, J = 5.2 Hz, 2H, H1), 8.23 (s, 1H, Hf), 7.53 (m, 5H, H3, H6, H7, H10, H11), 7.41 (d, J = 5.6 Hz, 2H, H2), 7.08 (m, 5H, H4, H5, H8, H9, H12). ^{13}C NMR (100 MHz, DMSO-d_6, ppm): δ 154.10 (CO), 152.79 (CO), 150.06 (CO), 146.71 (C), 131.47 (C), 131.31 (C), 131.26 (C), 131.25 (C), 130.79 (C), 124.50 (CH), 124.48 (CH), 124.42 (CH), 124.35 (CH), 124.27 (CH), 124.25 (CH), 124.18 (CH), 124.17 (CH), 124.15 (CH), 124.09 (CH), 124.06 (CH), 112.24 (CH). ESI-MS: m/z, 100%, 907.3435 $[M+Na]^+$ (calcd. for 907.3147).

S3. Synthetic Procedures of *cis*-Platinum(II) Complexes

cis-$Pt(PEt_3)_2Cl_2$: Triethylphosphine (0.71 g, 6 mmol) and potasium tetrachloroplatinate (II) (K_2PtCl_4, 0.83 g, 2 mmol) were dissolved in dichloromethane (20 mL) under argon. After the reaction mixture was stirred at room temperature for 12 hours, the colorless solids were precipitated and separated by filtration. Then, the filtrate solution was concentrated under reduced pressure, and a white crude product was observed. White flake crystals of *cis*-$Pt(PEt_3)_2Cl_2$ were obtained by recrystallization of the crude product in acetonitrile. 0.71 g, yield: 71%. ^{1}H NMR (400 MHz, DMSO-d_6, ppm): δ 1.81 (m, J = 8.0 Hz, 6H, CH_2), 1.10 (m, J = 8.0 Hz, 9H, CH_3).

cis-$Pt(PEt_3)_2SO_4$: To a solution (CH_2C1_2, 40 mL) of of $Pt(PEt_3)_2(Cl)_2$ (1.0 g, 2 mmol), Ag_2SO_4 (1.87 g, 6 mmol) was added. The reaction mixture was allowed to stir at room temperature for 12 h in dark. The heterogeneous mixture was filtered, and the solidts were obtained. Then, the solids were washed several times with diethyl ether and dried under vacuum to yield *cis*-$Pt(PEt_3)_2(SO_4)_2$ as a white solid. 0.59 g, yield: 56%. ^{1}H NMR (400 MHz, DMSO-d_6, ppm): δ 1.88 (m, J = 8.0 Hz, 6H, Hh), 1.09 (m, J = 8.0 Hz, 9H, Hg). ESI-MS: m/z, 100%, 742.6576 $[(Pt(PEt_3)_2)_3(SO_4)_2]^{2-}$ (calcd. for 742.6711).

Pt(II) acceptors *cis*-$Pt(PEt_3)_2Cl_2$ and *cis*-$Pt(PEt_3)_2(OTf)_2$ were prepared according to previously reported procedures (*J. Am. Chem. Soc.* **1995**, *117*, 6273–6283).

S4. Assembly Driven by Cooperative Anion Coordination and Cation Coordination

Supercoils $Pt_2\mathbf{L^1}_2(SO_4)_2$: The ligand $\mathbf{L^1}$ (1.3 mg, 1.5 mmol) was completely dissolved in 500 μL DMSO-d_6 solution, and then 1 equivalent *cis*-$Pt(PEt_3)_2SO_4$ was added to the solution. After stirring at room temperature for 1 h and a trace amount of insoluble material was filtrated. The metallacycle $Pt_2\mathbf{L^1}_2(SO_4)_2$ was demonstrated by ^{1}H NMR spectroscopy. ^{1}H NMR (400 MHz, DMSO-d_6, ppm): δ 10.66 (s, 1H, Ha), 9.40 (s, 1H, Hb), 9.38 (s, 1H, Hc), 9.31 (s, 1H, Hd), 9.21 (s, 1H, He), 8.96 (d, 1H, Hf), 8.41 (m, 1H, H1), 7.86 (m, 3H, H3, H7), 7.73 (m, 1H, H4), 7.51 (m, 3H, H2, H6), 7.11 (m, 5H, H5, H8, H10, H11, H12), 6.58 (t, 1H, H9), 1.70 (m, 6H, Hh), 1.13 (m, 9H, Hg). ESI-MS: m/z 1434.9995 $[M + 2Na]^{2+}$ (calcd. for 1434.9144).

Supercoils $Pt_2\mathbf{L^1}_2(OTf)_4$: The ligand $\mathbf{L^1}$ (2.2 mg, 2.5 μmol) was completely dissolved in 500 μL DMSO-d_6 solution, and then 1 equivalent of $[Pt(PEt_3)_2](OTf)_2$ was added to the solution. After stirring at room temperature for 1 h. The assembled structure was characterized by ^{1}H NMR

spectroscopy and Mass spectrometry. ^{1}H NMR (400 MHz, DMSO-d_6, ppm): δ 10.15 (s, 1H, Ha), 8.60 (d, 2H, H1), 8.51 (s, 1H, Hb), 8.48 (s, 1H, Hc), 8.46 (s, 1H, Hd), 8.36 (d, 1H, He), 8.29 (s, 1H, Hf), 7.55 (m, 4H, H2, H3, H4), 7.47 (m, 3H, H6, H7, H10), 7.14 (m, 2H, H11, H12), 7.00 (m, 3H, H5, H8, H9), 1.75 (m, 6H, Hh), 1.17 (m, 9H, Hg). ESI-MS: m/z 1464.9145, $[M - 2OTf]^{2+}$ (calcd. for 1464.9249).

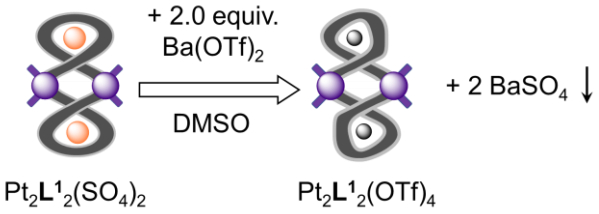

Preparation of $Pt_2\mathbf{L^1}_2(OTf)_4$ by anion exchange: To a solution of $Pt_2\mathbf{L^1}_2(SO_4)_2$ (2.8 mg, 1.0 μmol) in DMSO-d_6 (0.5 mL), two equivalent of $Ba(OTf)_2$ (4 μL, taken from a prepared stock solution (500 mM) in water) was added. White powder was observed to precipitate immediately, the solution was collected by centrifugation and filtration. The obtained solution was further characterized and confirmed to be the $Pt_2\mathbf{L^1}_2(OTf)_4$ complex by ^{1}H NMR and MS.

Supercoils $Pt_2\mathbf{L^2}_2(SO_4)_2$: The ligand $\mathbf{L^2}$ (2.3 mg, 3.0 μmol) was completely dissolved in 500 μL DMSO-d_6 solution, and then 1 equivalent of *cis*-$Pt(PEt_3)_2SO_4$ was added to the solution. After stirring at room temperature for 1 h and a trace amount of insoluble material was filtrated. The metallacycles $Pt_2\mathbf{L^2}_2(SO_4)_2$ were demonstrated by ^{1}H NMR spectroscopy. ^{1}H NMR (400 MHz, DMSO-d_6, ppm): δ 10.83 (s, 1H, Ha), 9.49 (s, 1H, Hb), 9.04 (s, 3H, Hc, Hd, He), 7.95 (m, 3H, H7, H8, H10), 7.91 (d, 2H, H1), 7.81 (m, 2H, H3, H6), 7.13 (m, 2H, H5, H9), 7.00 (m, 3H, H2, H4), 1.70 (m, 6H, Hh), 1.13 (m, 9H, Hg). ESI-MS: m/z 1229.9054 $[M - SO_4]^{2+}$ (calcd. for 1229.9008), m/z 1300.8734 $[M + 2Na]^{2+}$ (calcd. for 1300.8663).

Supercoils $Pt_2\mathbf{L^2}_2(OTf)_4$: The ligand $\mathbf{L^2}$ (1.9 mg, 2.5 μmol) was completely dissolved in 500 μL DMSO-d_6 solution, and then 1 equivalent $[Pt(PEt_3)_2](OTf)_2$ was added to the solution. After stirring at room temperature for 1 h. The assembled structure was characterized by ^{1}H NMR spectroscopy and Mass spectrometry. ^{1}H NMR (400 MHz, DMSO-d_6, ppm): δ 10.23 (s, 1H, Ha), 8.75 (s, 1H, Hb), 8.62 (s, 1H, Hc), 8.57 (d, 2H, H1), 8.41 (s, 1H, Hd), 8.34 (d, 1H, He), 7.54 (m, 5H, H2, H3, H4, H7), 7.31 (d, 1H, H6), 7.20 (t, 1H, H5), 7.09 (m, 3H, H8, H9, H10), 1.78 (m, 6H, Hh), 1.16 (m, 9H, Hg). ESI-MS: m/z 1330.3966, $[M - 2OTf]^{2+}$ (calcd. for 1330.3760).

$Pt_2\mathbf{L^3}_2(OTf)_4$: The ligand $\mathbf{L^3}$ (1.9 mg, 2.8 μmol) was completely dissolved in 500 μL DMSO-d_6 solution, and then 1 equivalent $[Pt(PEt_3)_2](OTf)_2$ was added to the solution. After stirring at room temperature for 1 h. The assembled structure was characterized by ^{1}H NMR spectroscopy and Mass spectrometry. ^{1}H NMR (400 MHz, DMSO-d_6, ppm): δ 10.23 (s, 1H, Ha), 8.56 (s, 2H, Hb, Hc), 8.46 (s, 1H, Hd), 8.44 (d, 2H, H1), 7.66 (m, 3H, H2, H3), 7.56 (m, 2H, H6, H7), 7.23 (m, 1H, H4), 7.11 (m, 1H, H5), 7.05 (m, 1H, H8), 1.81 (m, 6H, Hh), 1.17 (m, 9H, Hg). ESI-MS: m/z 1196.3506, $[M - 2OTf]^{2+}$ (calcd. for 1196.3279).

S5. X-ray Diffraction Data

Crystal $(TBA)_2[\mathbf{L^1}\bullet SO_4]$: $(TBA)_2SO_4$ solution (9 μL, 0.625 mol/L, in water) was added to a suspension of $\mathbf{L^1}$ (5.0 mg, 5.7 μmol) in mixed solution of acetone and acetonitrile. After stirring overnight at room temperature, a colorless solution was obtained. Slow vapor diffusion of diethyl ether into this solution provided colorless crystals of $(TBA)_2[\mathbf{L^1}\bullet SO_4]$ within one week. The crystal was directly mounted on a diffractometer for data collection.

Crystal $(TPA)_2[\mathbf{L^2}\bullet SO_4]$: $(TPA)_2SO_4$ solution (10 μL, 0.625 mol/L, in acetonitrile) was added to a suspension of $\mathbf{L^2}$ (5 mg, 6.6 μmol) in acetone. After stirring overnight at room temperature, a clearly colorless solution was obtained. Slow vapor diffusion of diethyl ether into this solution provided yellow crystals of $(TPA)_2[\mathbf{L^2}\bullet SO_4]$ within two weeks. The crystal was directly mounted on a diffractometer for data collection.

Crystal $(TEA)_2[\mathbf{L^3}\bullet SO_4]$: $(TEA)_2SO_4$ solution (10 μL, 0.625 mol/L, in acetonitrile) was added to a suspension of $\mathbf{L^3}$ (5 mg, 8.1 μmol) in acetone. After stirring overnight at room temperature, a clearly colorless solution was obtained. Slow vapor diffusion of diethyl ether into this solution provided yellow crystals of $(TEA)_2[\mathbf{L^3}\bullet SO_4]$ within two weeks. The crystal was directly mounted on a diffractometer for data collection.

Crystal $Pt_2\mathbf{L^1}_2(SO_4)_2$: The ligand $\mathbf{L^1}$ (3 mg, 3.4 μmol) was completely dissolved in 1 mL mixture solution of DMSO and DMF (v/v: DMSO/DMF = 7:3), and then 1 equivalent of *cis*-$Pt(PEt_3)_2SO_4$ was added to the above clear solution. The clarified solution was obtained after stirring at room temperature for 1 h. Colorless crystals of $[Pt_2\mathbf{L^1}_2](SO_4)_2$ were obtained by slow vapor diffusion of acetone into this solution within one month. The crystal was directly mounted on a diffractometer for data collection.

Crystal $Pt_2\mathbf{L^2}_2(SO_4)_2$: The ligand $\mathbf{L^2}$ (1.50 mg, 2.0 μmol) was completely dissolved in 1 mL DMF solution, and then 1 equivalent of *cis*-$Pt(PEt_3)_2SO_4$ was added to the above clear solution. After stirring at room temperature for 1 h, a trace amount of insoluble material was filtrated. Colorless crystals of $Pt_2\mathbf{L^2}_2(SO_4)_2$ were obtained by slow vapor diffusion of acetone into the clear solution within two weeks. The crystal was directly mounted on a diffractometer for data collection.

Crystal $Pt_2\mathbf{L^3}_2(SO_4)_2$: The ligand $\mathbf{L^3}$ (1.50 mg, 2.5 μmol) was completely dissolved in 1 mL DMF solution, and then 1 equivalent of *cis*-$Pt(PEt_3)_2SO_4$ was added to the above clear solution. After stirring at room temperature for 1 h, a trace amount of insoluble material was filtrated. Colorless crystals of $Pt_2\mathbf{L^3}_2(SO_4)_2$ were obtained by slow vapor diffusion of acetone into the clear solution within two weeks. The crystal was directly mounted on a diffractometer for data collection.

X-ray diffraction data of the crystal foldamers of $(TBA)_2[\mathbf{L^1}\bullet SO_4]$, $(TEA)_2[\mathbf{L^3}\bullet SO_4]$, $(TPA)_2[\mathbf{L^2}\bullet SO_4]$, and structures of $[Pt_2\mathbf{L^3}_2](SO_4)_2$, $Pt_2\mathbf{L^2}_2(SO_4)_2\bullet(H_2O)_2$ were recorded on a Bruker D8 Venture Photon II diffractometer with graphite-monochromatic Mo Kα radiation (λ = 0.71073 Å) under 150 K. X-ray diffraction data of the crystals metallacycle $Pt_2\mathbf{L^1}_2(SO_4)_2\bullet(H_2O)_4$ were detected on a Bruker APEX-II CCD diffractometer with graphite-monochromatic GaK radiation (λ = 1.34139 Å) under 150 K. An empirical absorption correction using SADABS was applied for all data. (SADABS v 2018. 1, Bruker AXS, Madison, WI, **2018**.) The structures were solved by the dual methods *via* SHELXS program. (A short history of SHELX, G. M. Sheldrick, *Acta Cryst.* **2008**, A*64*, 112-122). All structures were solved and refined to convergence by the full-matrix least-squares on F^2 for all independent reflections using the program SHELXL. Hydrogen atoms were included in idealized positions with thermal parameters equivalent to 1.2 times those of the atom to which they were attached. All the crystal structures have been deposited with the Cambridge Crystallographic Data Centre (CCDC), and their corresponding CCDC numbers are shown in Table S1 and S2.

Table S1. Crystal data and refinement details of foldamers

Complexes	$(TEA)_2[\mathbf{L^3}\bullet SO_4]$	$(TPA)_2[\mathbf{L^2}\bullet SO_4]$	$(TBA)_2[\mathbf{L^1}\bullet SO_4]$
CCDC Number	2395072	2394995	2395079
Formula	$C_{51.50}H_{48}N_{12}O_9S$	$C_{69}H_{96}N_{15}O_{11}S$	$C_{170.23}H_{233.22}N_{32}O_{24}\ S_2$
M	1011.08	1343.66	3175.97
Crystal system	Triclinic	Monoclinic	Triclinic
Space group	P-1	$P2_1/c$	P-1
a (Å)	13.250(7)	19.753(6)	13.359(0)
b (Å)	13.738(8)	24.387(8)	23.155 (5)
c (Å)	16.309(2)	15.609(5)	29.583(0)
α (deg)	74.178	90	84.857(2)
β (deg)	88.822	107.215	89.750(2)
γ (deg)	67.602	90	79.274(0)
V (Å^3)	2629	7182	8954
Z	2	4	2
T (K)	150	150	150
D_{calc} (g·cm^{-3})	1.277	1.243	1.178
R(int)	0.0359	0.0820	0.0510
GOF	1.056	1.100	1.088
$R1$ [$I > 2\sigma(I)$]	0.0828	0.0819	0.1045
$wR2$ [$I > \sigma(I)$]	0.2412	0.2470	0.3269

Table S2. Crystal data of co-assembled structures by anion-metal coordination.

Complexes	$Pt_2\mathbf{L^3}_2(SO_4)_2$	$Pt_2\mathbf{L^2}_2(SO_4)_2{\bullet}(H_2O)_2$	$Pt_2\mathbf{L^1}_2(SO_4)_2{\bullet}(H_2O)_4$
CCDC Number	2394994	2394496	2394489
Formula	$C_{53}H_{73}N_{13}O_{11}P_2PtS$	$C_{123}H_{180}N_{30}O_{28}P_4Pt_2S_2$	$C_{124}H_{144}N_{28}O_{30}P_4Pt_2S_6$
M	1357.33	3105.14	3213.08
Crystal system	Triclinic	Orthorhombic	Orthorhombic
Space group	*P*-1	*Pbcn*	*Pccn*
a (Å)	13.459(1)	20.263(8)	19.910(5)
b (Å)	16.160(9)	19.988(5)	42.714(4)
c (Å)	18.985(2)	33.454(3)	16.646(1)
α (deg)	91.800°	90°	90°
β (deg)	97.120°	90°	90°
γ (deg)	105.492°	90°	90°
V (Å^3)	3939.7(8)	13550.3(19)	14156.8(18)
Z	2	4	4
T (K)	180	191	150
D_{calc} (g·cm^{-3})	1.144	1.522	1.237
R(int)	0.1411	0.0712	0.0798
GOF	0.995	1.1170	1.043
R_1 [$I > 2\sigma(I)$]	0.0662	0.0464	0.0713
wR_2 [$I > \sigma(I)$]	0.1707	0.1435	0.2096

Table S3. Hydrogen bond parameters in the crystal structure of $(TEA)_2[\mathbf{L^3}\bullet SO_4]$.

D-H· · · A	d(D-H)	d(H· · · A)	d(D· · · A)	∠(DHA)
N2-H2· · · O7	0.88	1.96	2.799(6)	158
N3-H3· · · O7	0.88	2.07	2.876(5)	152
N4-H4· · · O5	0.88	2.34	3.089(5)	143
N5-H5· · · O5	0.88	1.96	2.809(5)	163
N6-H6· · · O8	0.88	2.08	2.890(5)	152
N7-H7· · · O8	0.88	2.00	2.833(5)	157
N8-H8· · · O6	0.88	2.05	2.886(5)	158
N9-H9· · · O6	0.88	2.19	3.004(6)	153
N9-H9· · · O7	0.88	2.46	3.177(5)	139

Table S4. Hydrogen bond parameters [Å and °] in the crystal structure of $(TPA)_2[\mathbf{L^2}\bullet SO_4]$.

D-H···A	d(D-H)	d(H···A)	d(D···A)	∠(DHA)
N2-H2···O6	0.86	2.17	3.008(3)	165
N3-H···O6	0.86	2.33	3.121(3)	152
N4-H4···O7	0.86	2.58	3.319(3)	144
N5-H5···O7	0.86	2.03	2.856(3)	161
N6-H6···O6	0.86	2.29	3.096(3)	155
N7-H7···O6	0.86	2.13	2.961(3)	162
N8-H8···O9	0.86	2.12	2.918(3)	155
N9-H9···O9	0.86	2.2	2.980(3)	150
N10-H10···O8	0.86	2	2.811(3)	156
N11-H11···O8	0.86	2.2	2.972(3)	149

Table S5. Hydrogen bond parameters [Å and °] in the crystal structure of $(TBA)_2[\mathbf{L^1}\bullet SO_4]$.

D-H···A	d(D-H)	d(H···A)	d(D···A)	∠(DHA)
N2-H2···O15	0.88	2.22	3.088(2)	169
N3-H3···O13	0.88	2.13	2.782(2)	130
N4-H4···O14	0.88	2.46	3.081(2)	128
N5-H5···O14	0.88	2.24	3.015(2)	147
N6-H6···O15	0.88	2.09	2.926(2)	159
N7-H7···O15	0.88	2.18	3.010(2)	157
N8-H8···O16	0.88	1.99	2.845(2)	164
N9-H9···O16	0.88	2.27	3.076(2)	152
N10-H10···O13	0.88	2.42	3.179(2)	144
N11-H11···O13	0.88	2.02	2.798(2)	147
N12-H12···O16	0.88	2.34	3.119(2)	148
N13-H13···O16	0.88	1.96	2.782(2)	155

Table S6. Hydrogen bond parameters [Å and °] in the crystal structure of $Pt_2\mathbf{L^3}_2(SO_4)_2$.

D-H···A	d(D-H)	d(H···A)	d(D···A)	∠(DHA)
N2-H2···O5	0.88	2.16	2.969(5)	153
N3-H3···O5	0.88	1.97	2.824(4)	162
N4-H4···O6	0.88	2.09	2.894(4)	152
N5-H5···O6	0.88	2.1	2.898(4)	151
N6-H6···O7	0.88	2.01	2.848(4)	159
N7-H7···O7	0.88	2.12	2.950(4)	157
N8-H8···O8	0.88	2.01	2.847(5)	159
N9-H9···O8	0.88	2.34	3.113(6)	146

Table S7. Hydrogen bond parameters [Å and °] in the crystal structure of $Pt_2\mathbf{L^2}_2(SO_4)_2\bullet(H_2O)_2$.

D-H···A	d(D-H)	d(H···A)	d(D···A)	∠(DHA)
N2-H2···O9	0.88	2.06	2.838(6)	147
N3-H3···O9	0.88	2.15	2.938(6)	148
N4-H4···O10	0.88	2	2.863(6)	166
N5-H5···O10	0.88	2.43	3.211(6)	148
N6-H6···O7	0.88	2.33	2.962(6)	129
N7-H7···O8	0.88	2.09	2.965(7)	172
N8-H8A···O7	0.88	2.29	3.107(9)	154
N9-H9A···O7	0.88	2.21	3.052(8)	160
N10-H10···O6	0.88	2.24	3.103(7)	167
O10-H10C···O8	0.88	1.95	2.788(6)	161
N11-H11···O9	0.88	2.21	3.070(6)	164

Table S8. Hydrogen bond parameters [Å and °] in the crystal structure of $Pt_2\mathbf{L^1}_2(SO_4)_2\bullet(H_2O)_4$.

D-H···A	d(D-H)	d(H···A)	d(D···A)	∠(DHA)
N2-H2···O9	0.88	1.93	2.798(8)	167
N4-H4···O11	0.88	2.1	2.866(8)	145
N6-H6···O7	0.88	2.22	3.093(7)	173
N7-H7···O8	0.88	2.21	3.057(7)	161
N8-H8···O10	0.88	2.25	2.990(7)	142
N9-H9···O12	0.88	2.16	2.844(14)	134
N10-H10···O8	0.88	2.44	3.226(7)	148
N11-H11···O8	0.88	1.94	2.810(6)	170
N12-H12···O8	0.88	2.42	3.245(6)	156
N13-H13···O7	0.88	1.92	2.779(6)	164

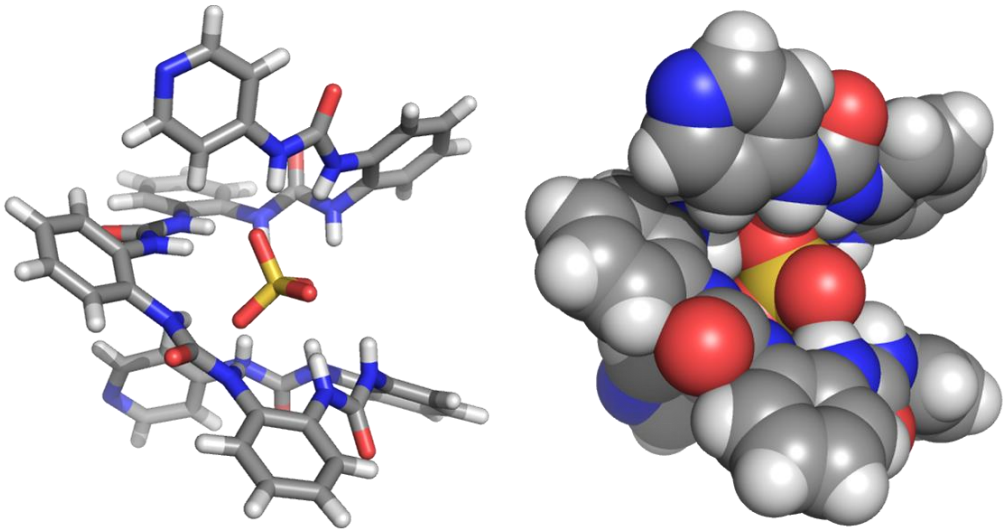

Figure S1. Single crystal structure of sulfate-coordinated foldamers based on ligand $\mathbf{L^1}$. Solvent molecules and tetrabutylammonium countercations are omitted for clarity. Racemic helix is observed in crystal, and only the left-handed conformation is illustrated. The distance between two terminal N atoms of the pyridyl group is 11.79(1) Å.

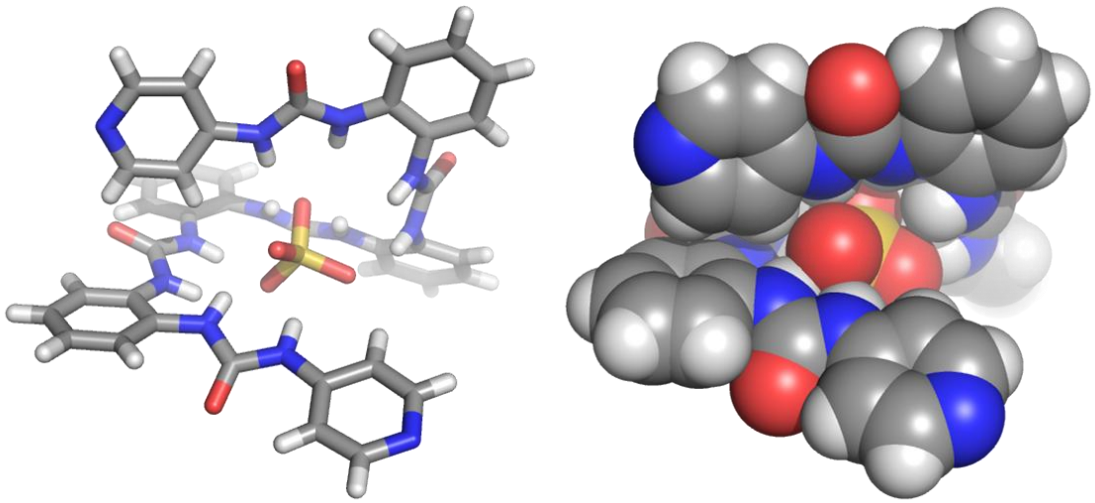

Figure S2. Single crystal structure of sulfate-coordinated foldamers based on ligand $\mathbf{L^2}$. Solvent molecules and tetrapropylammonium countercations are omitted for clarity. Racemic helix is observed in crystal, and only the left-handed conformation is illustrated. The distance between two terminal N atoms of the pyridyl group is 11.417(5) Å.

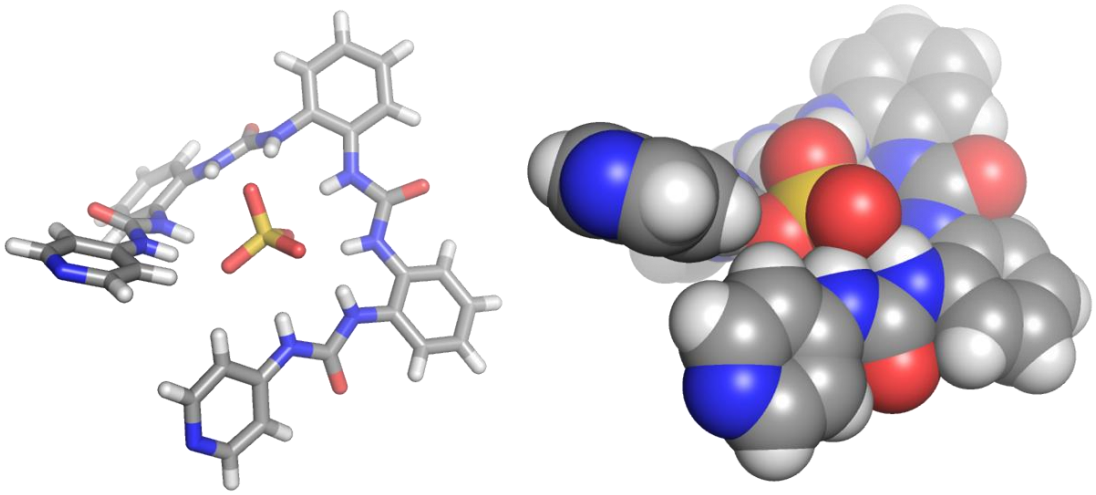

Figure S3. Single crystal structure of sulfate-coordinated foldamers based on ligand $\mathbf{L^3}$. Solvent molecules and tetraethylammonium countercations are omitted for clarity. Racemic helix is observed in crystal, and only the left-handed conformation is illustrated. The distance between two terminal N atoms of the pyridyl group is 6.697(8) Å.

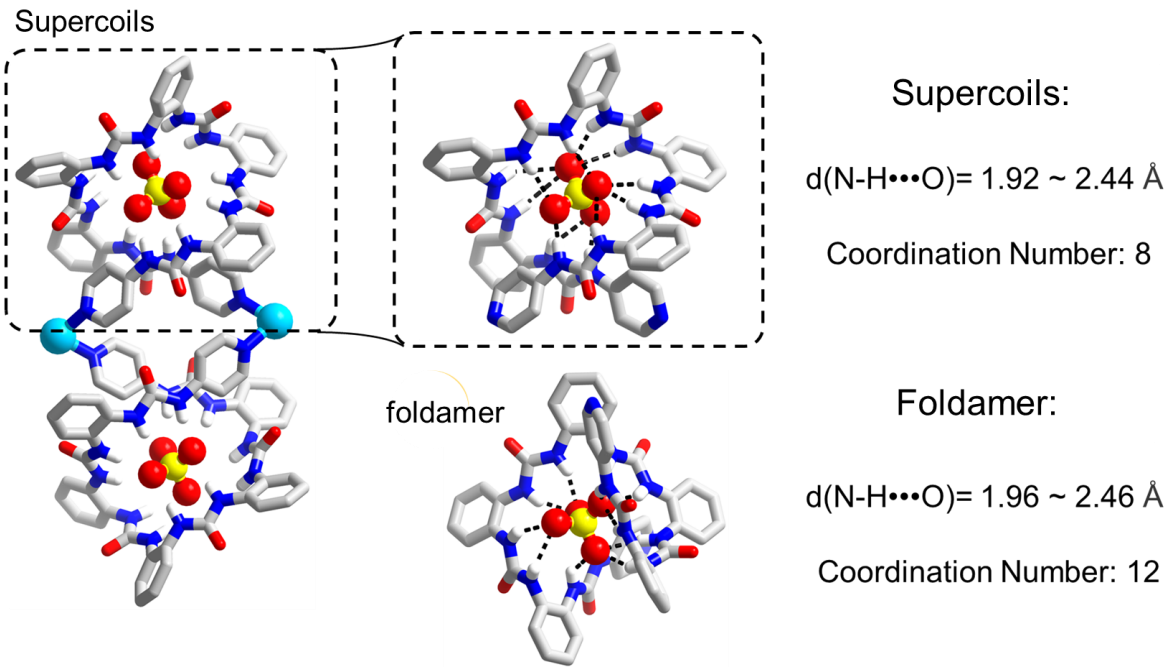

Figure S4. Comparison of hydrogen bonding networks as seen in the crystal structures of foldamer and supercoils made from the hexakisurea ligand $\mathbf{L^1}$.

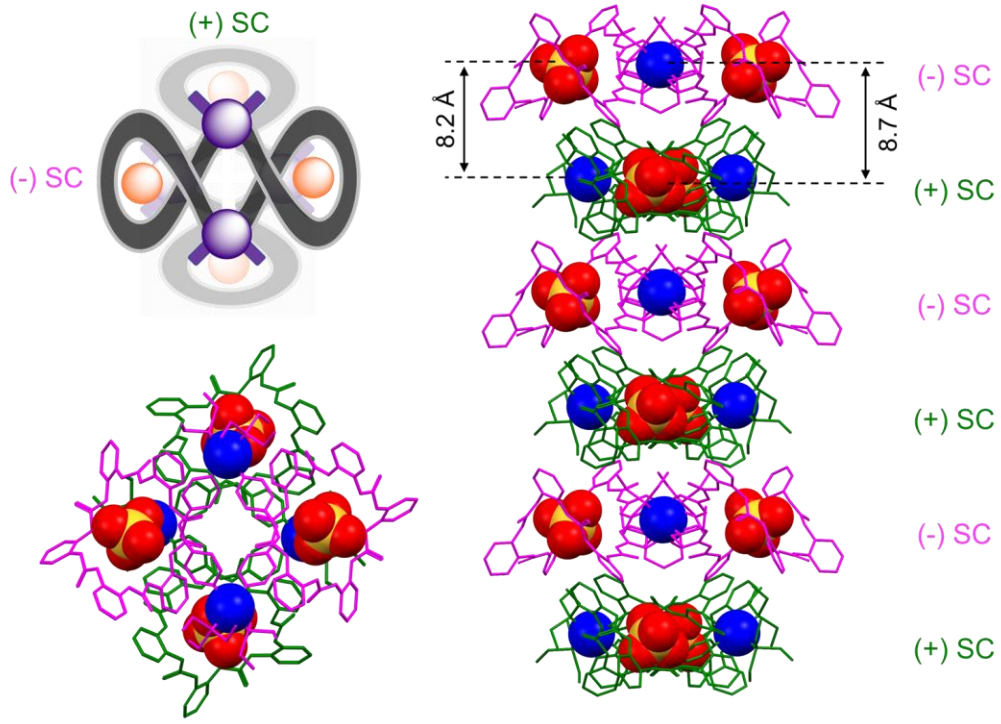

Figure S5. Packing structure of $\mathbf{L^1}$-based supercoils as seen in crystal.

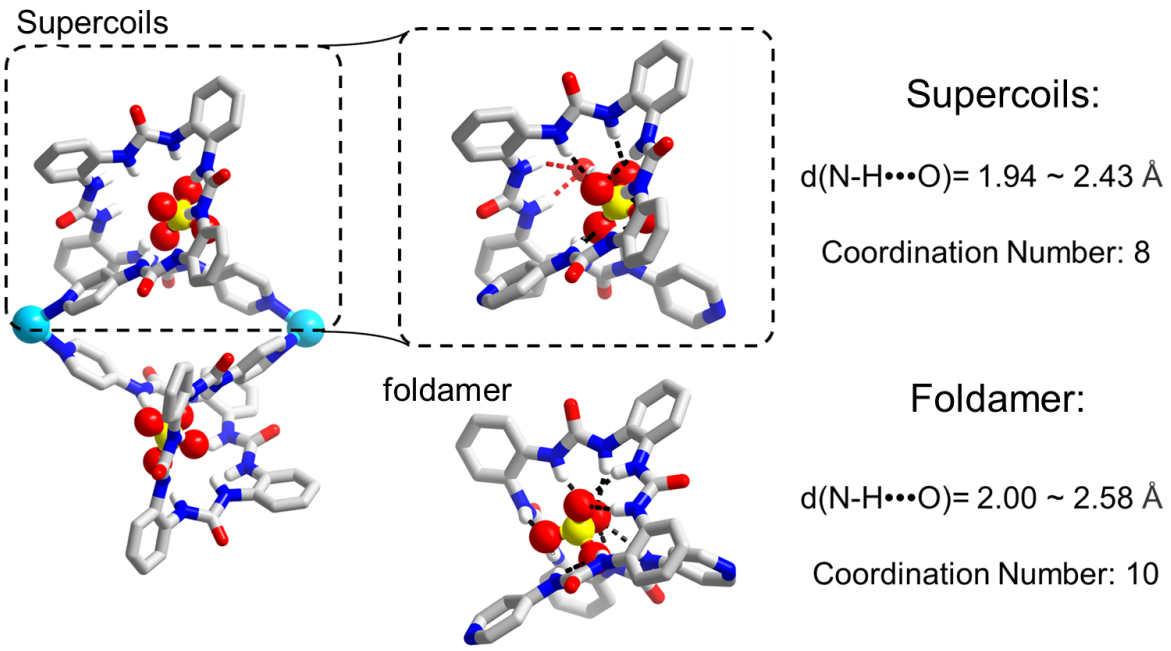

Figure S6. Comparison of hydrogen bonding networks as seen in the crystal structures of foldamer and supercoils made from the pentakisurea ligand **L**[2].

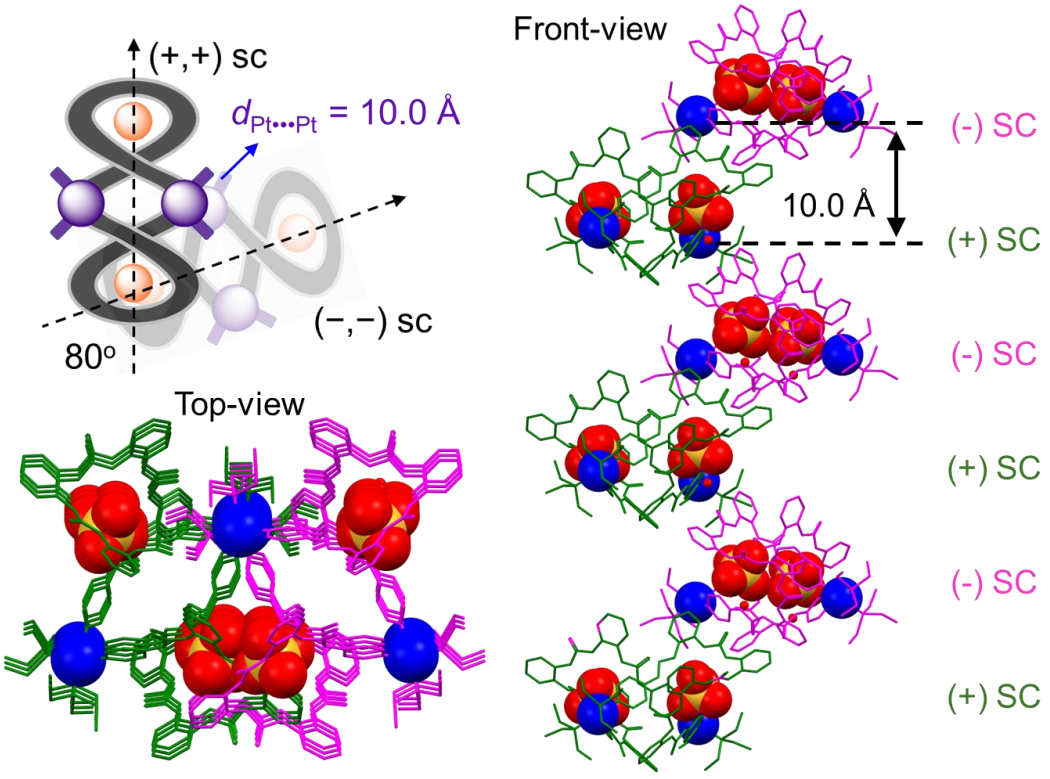

Figure S7. Packing structure of **L**[2]-based supercoils as seen in crystal.

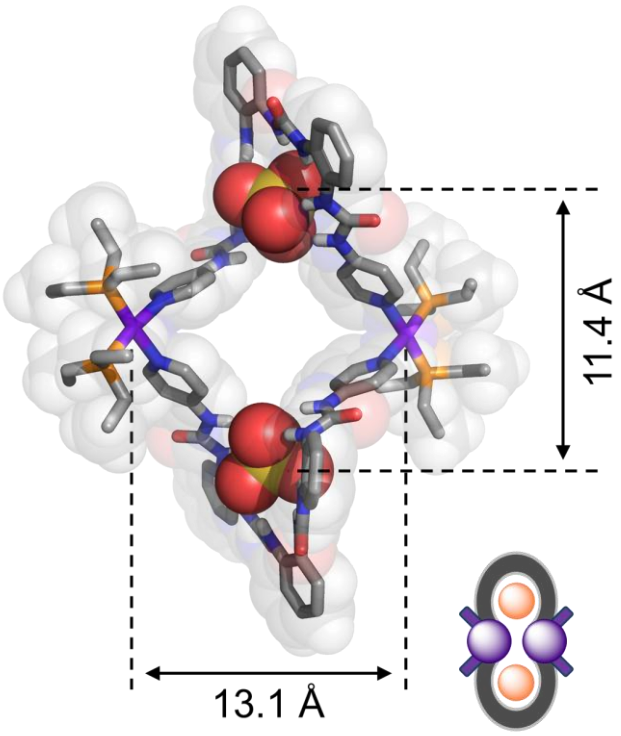

Figure S8. Single crystal structure of supramolecular macrocycle based on ligand **L**^{3}. Solvent molecules are omitted for clarity.

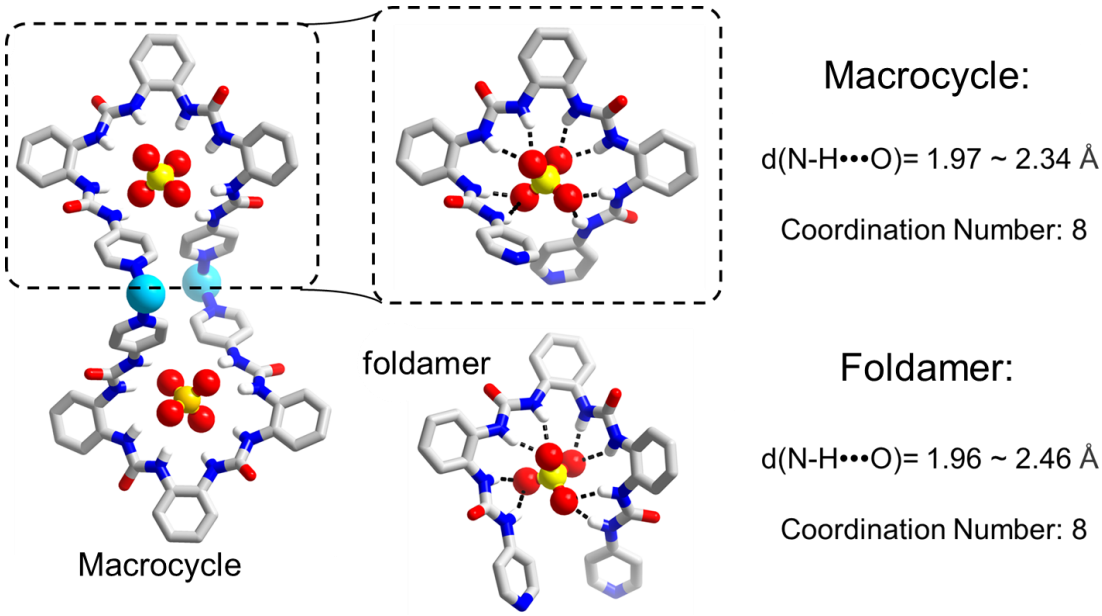

Figure S9. Comparison of hydrogen bonding networks as seen in the crystal structures of foldamer and supramolecular macrocycle made from the tetrakisurea ligand **L**^{3}.

S6. NMR and ESI-MS Results

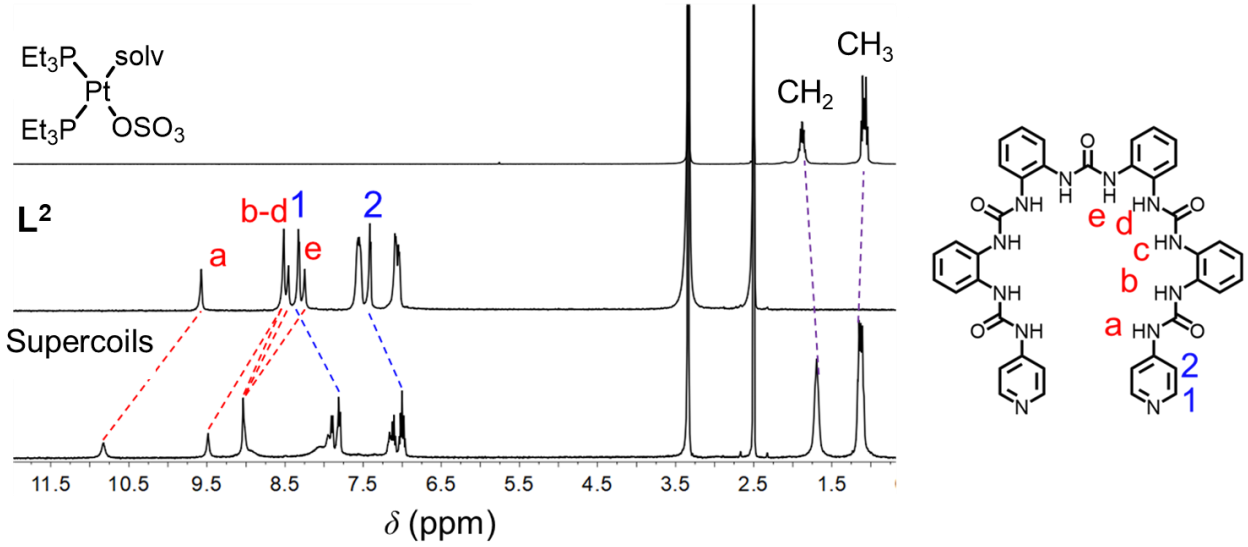

Figure S10. Stacked ^{1}H NMR spectra of *cis*-Pt(PEt$_3$)$_2$SO$_4$ (top), free ligand $\mathbf{L^2}$ (middle) and supercoils of Pt$_2$$\mathbf{L^2}$$_2$(SO$_4$)$_2$ (bottom), 1 mM, 400 MHz, DMSO-d_6, 298 K.

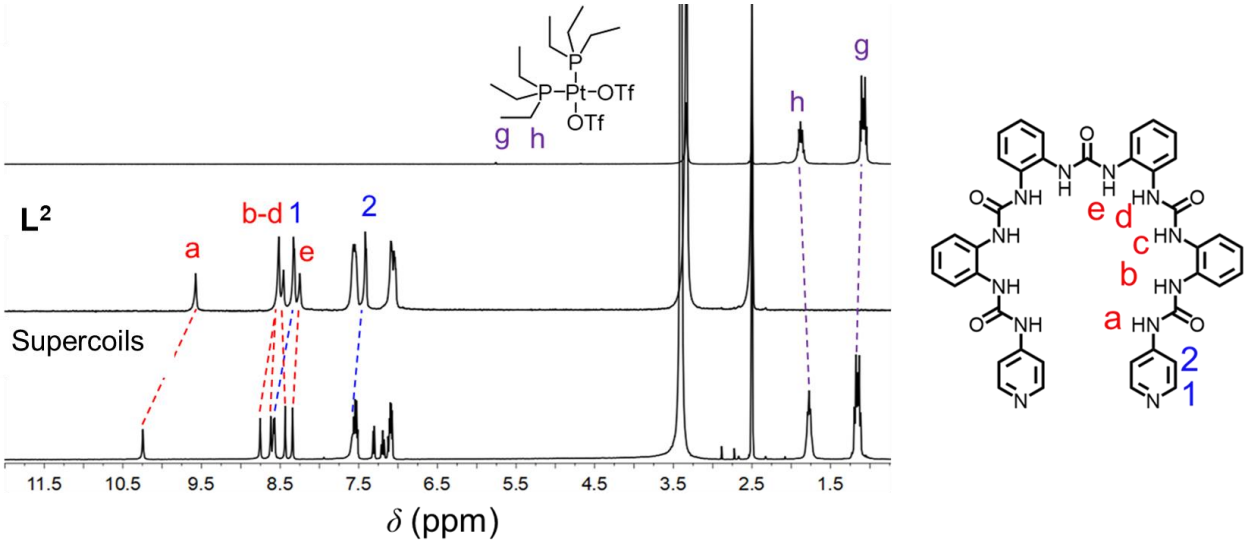

Figure S11. Stacked ^{1}H NMR spectra of *cis*- Pt(PEt$_3$)$_2$(OTf)$_2$ (top), free ligand $\mathbf{L^2}$ (middle) and supercoils of Pt$_2$$\mathbf{L^2}$$_2(OTf)_4$ (bottom), 1 mM, 400 MHz, DMSO-d_6, 298 K.

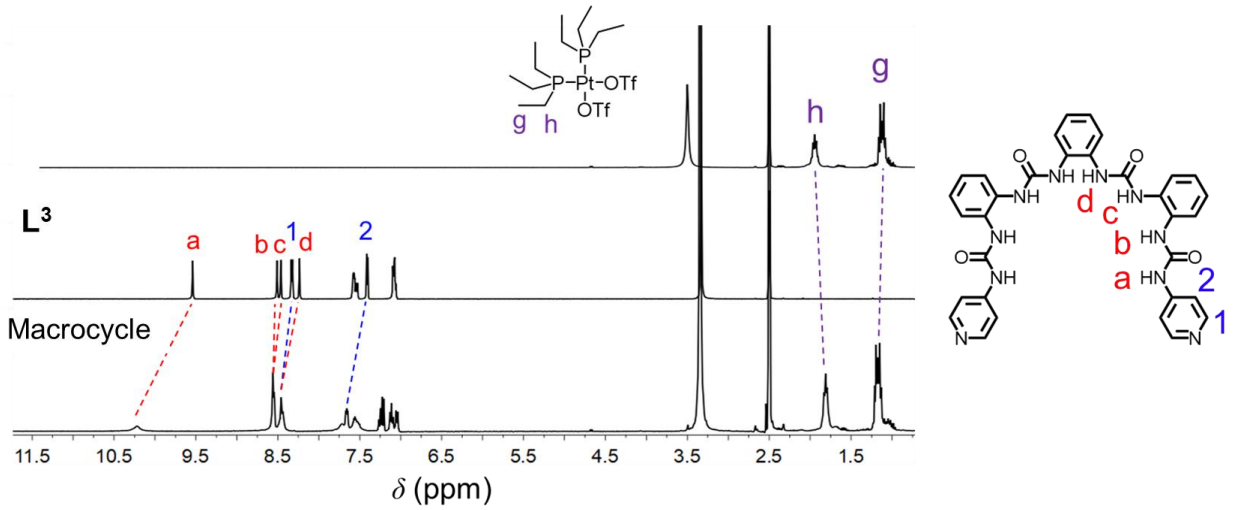

Figure S12. Stacked ^{1}H NMR spectra of *cis*-Pt(PEt$_3$)$_2$(OTf)$_2$ (top), free ligand **L^3** and metallacycle of Pt$_2$**L^3**$_2$(OTf)$_4$ (1 mM, 400 MHz, DMSO-d_6 , 298 K).

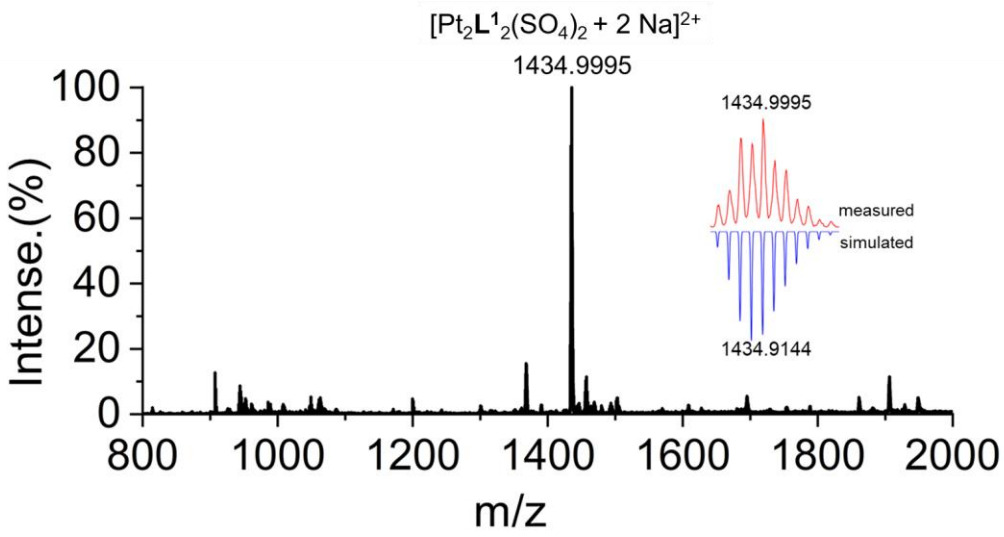

Figure S13. ESI-MS spectrum of Pt$_2$**L^1**$_2$(SO$_4$)$_2$ supercoils.

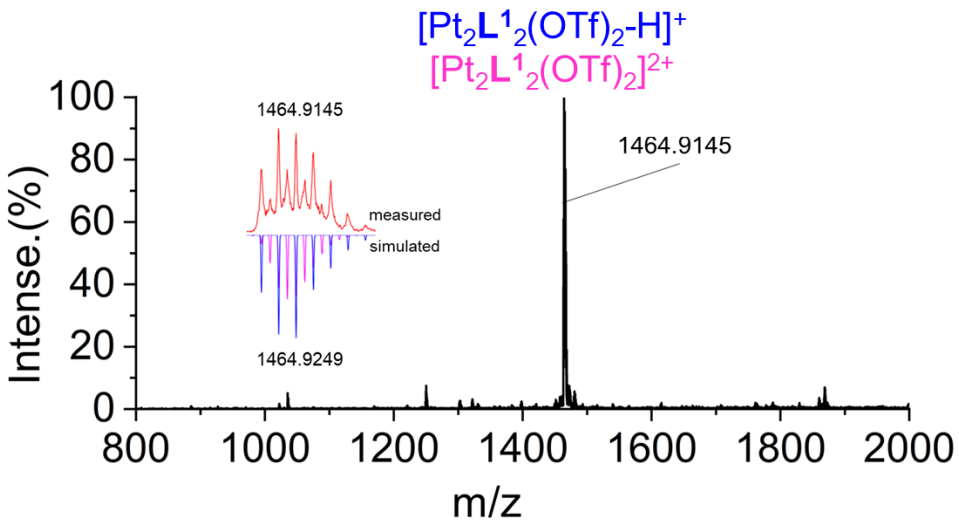

Figure S14. ESI-MS spectrum of $Pt_2\mathbf{L^1}_2(OTf)_4$ supercoils.

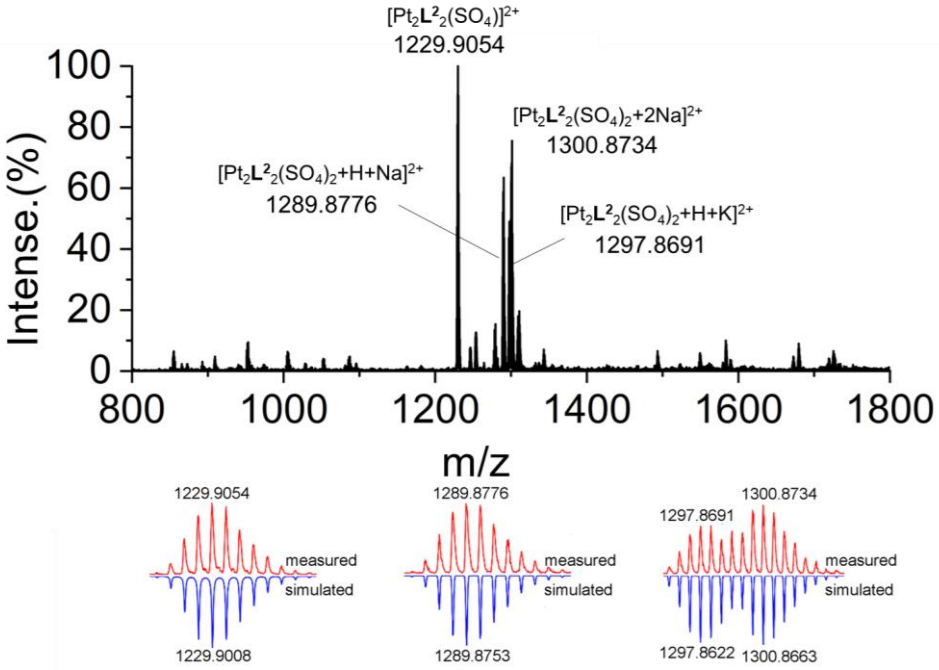

Figure S15. ESI-MS spectrum of $Pt_2\mathbf{L^2}_2(SO_4)_2$ supercoils.

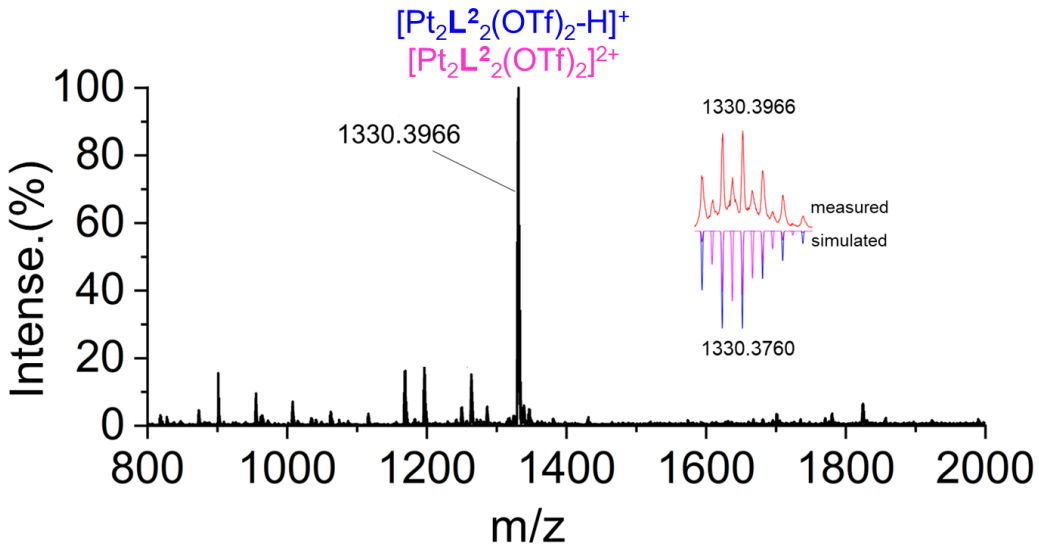

Figure S16. ESI-MS spectrum of $Pt_2\mathbf{L}^2{}_2(OTf)_4$ supercoils.

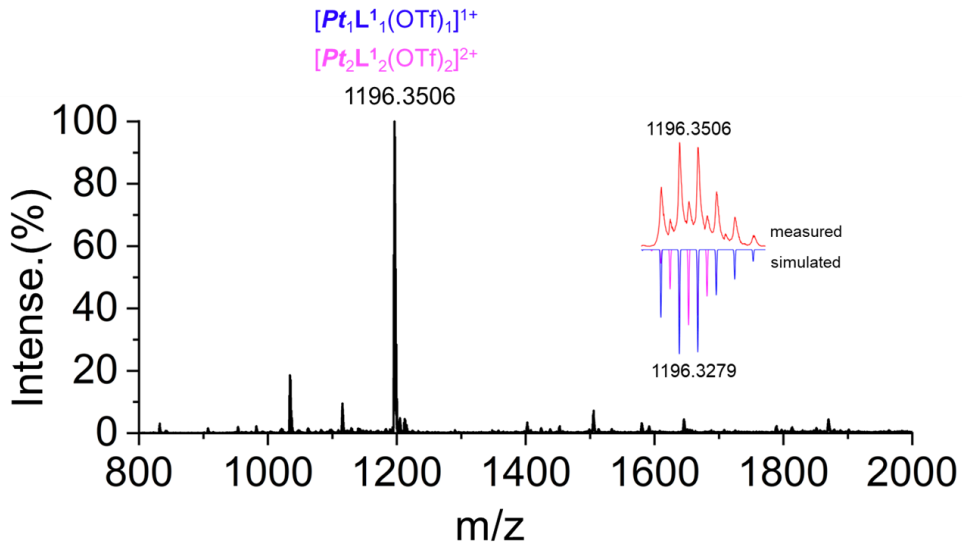

Figure S17. ESI-MS spectrum of $Pt_2\mathbf{L}^3{}_2(OTf)_4$ complex.

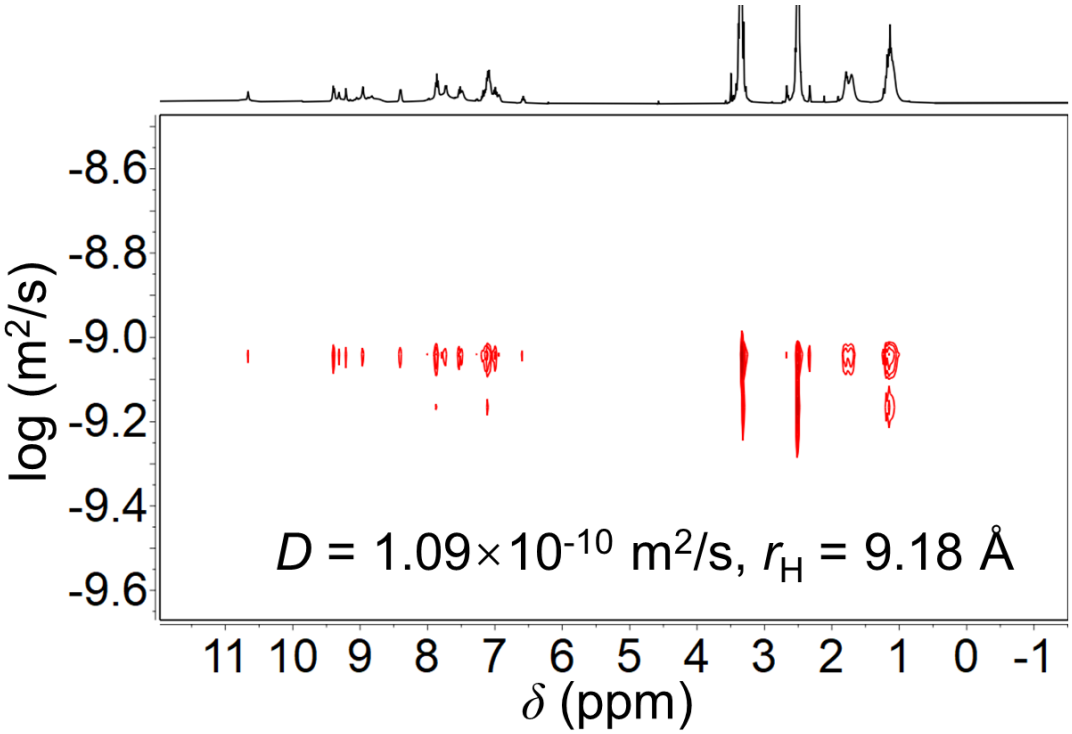

Figure S18. 2D DOSY spectrum for the $Pt_2\mathbf{L}^1_2(SO_4)_2$ supercoils (2 mM, 400 MHz, DMSO-d_6, 298 K).

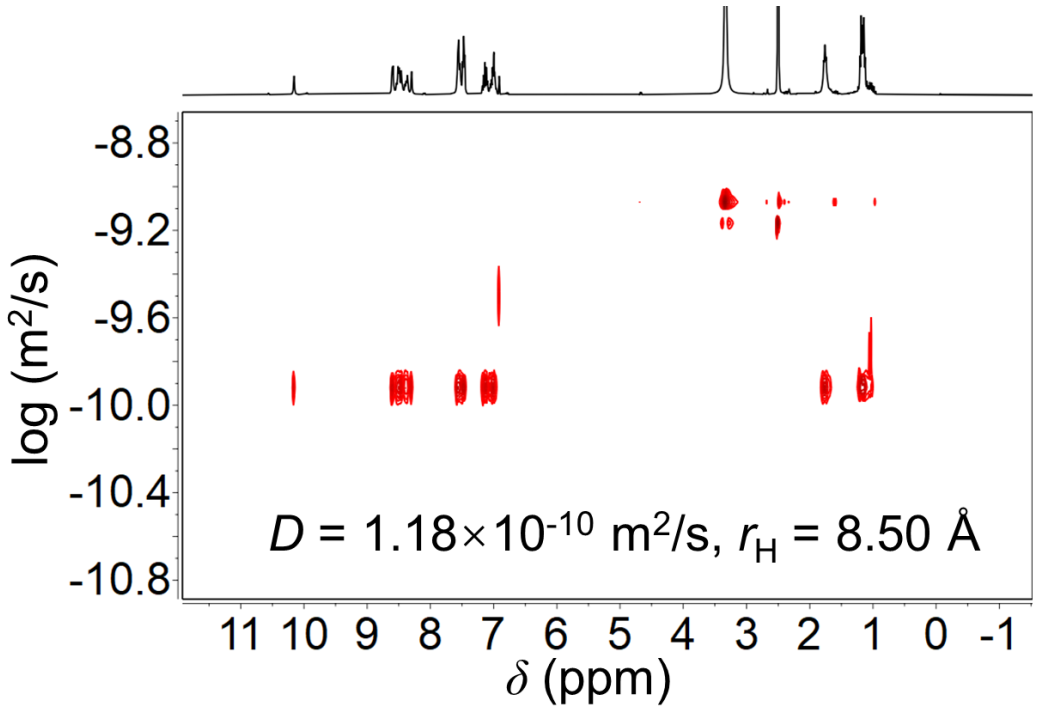

Figure S19. 2D DOSY spectrum for the $Pt_2\mathbf{L}^3_2(OTf)_4$ supercoils (2 mM, 400 MHz, DMSO-d_6, 298 K).

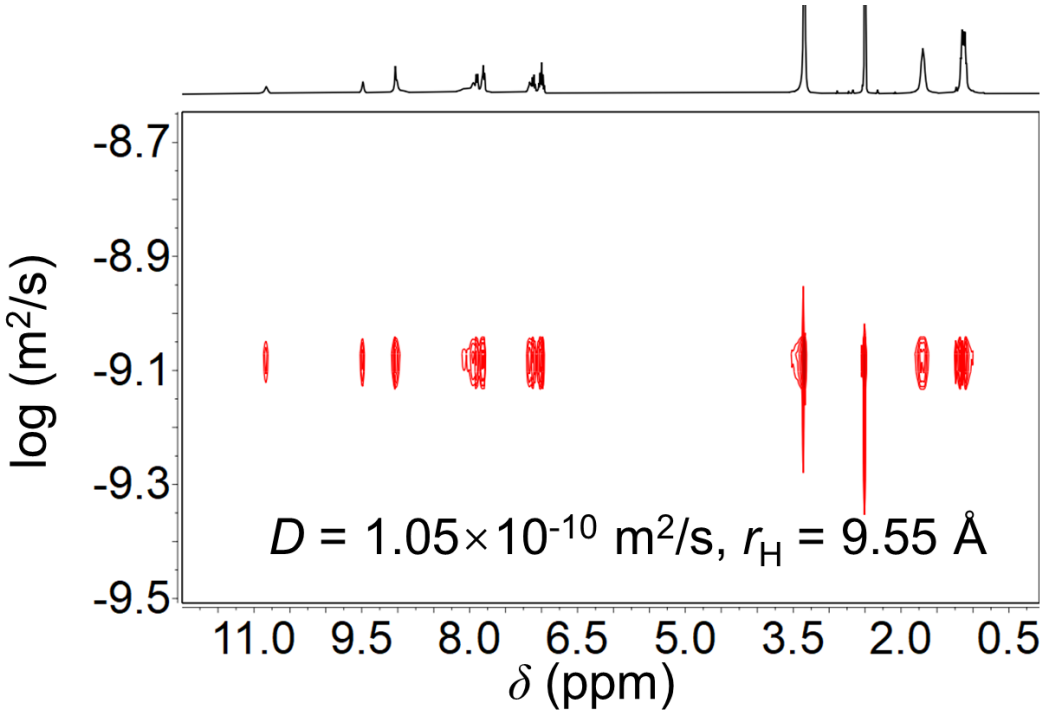

Figure S20. 2D DOSY spectrum for the $Pt_2\mathbf{L}^2_2(SO_4)_2$ supercoils (2 mM, 400 MHz, DMSO-*d*$_6$, 298 K).

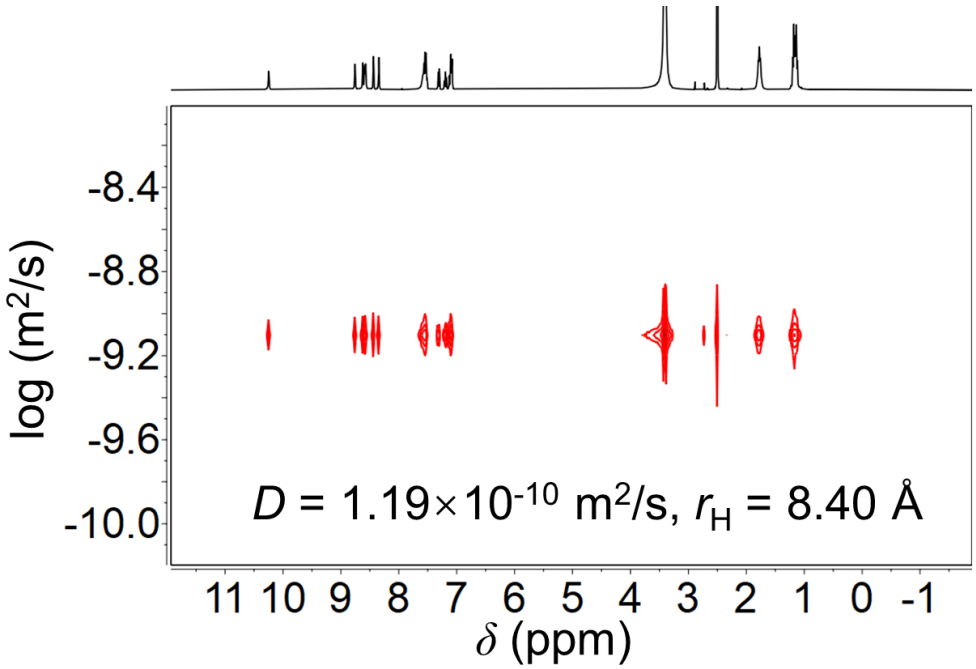

Figure S21. The DOSY spectrum for the $Pt_2\mathbf{L}^2_2(OTf)_4$ supercoils (2 mM, 400 MHz, DMSO-*d*$_6$, 298 K).

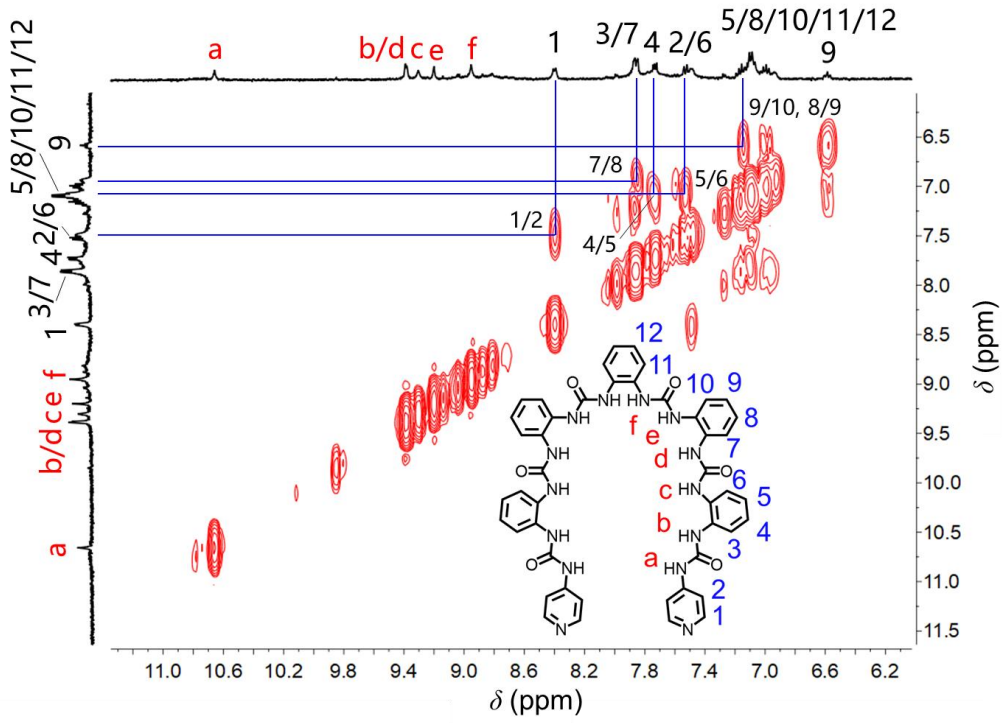

Figure S22. The ^{1}H-^{1}H COSY spectrum of $Pt_2\mathbf{L^1}_2(SO_4)_2$ (2 mM, 400 MHz, DMSO-d_6, 298 K).

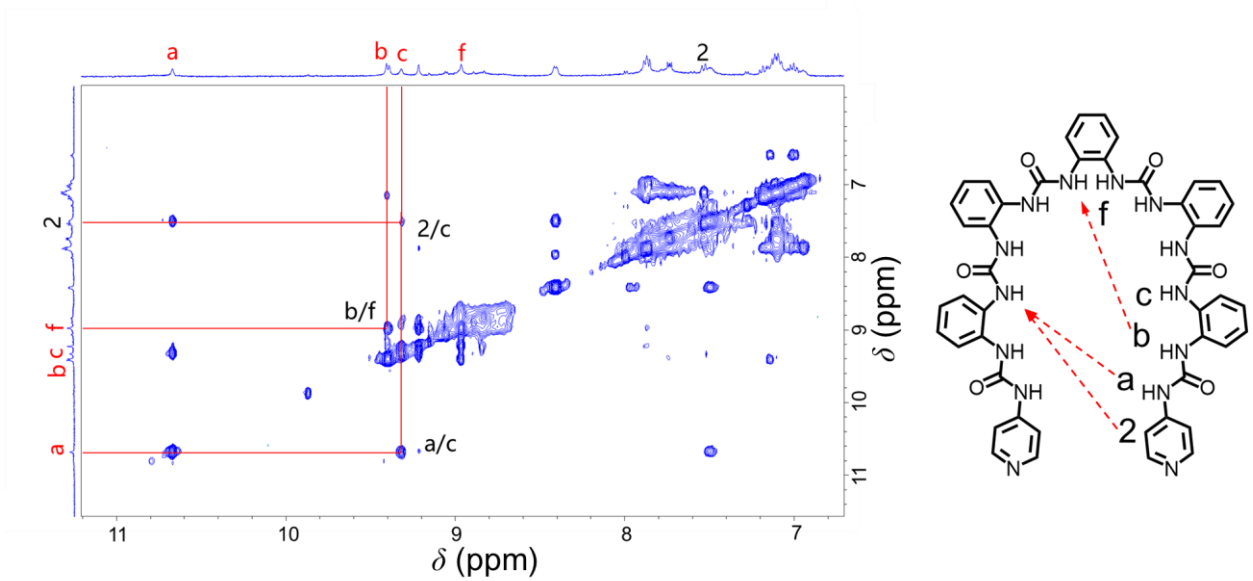

Figure S23. The ^{1}H-^{1}H NOESY spectrum of $Pt_2\mathbf{L^1}_2(SO_4)_2$ (2 mM, 400 MHz, DMSO-d_6, 298 K).

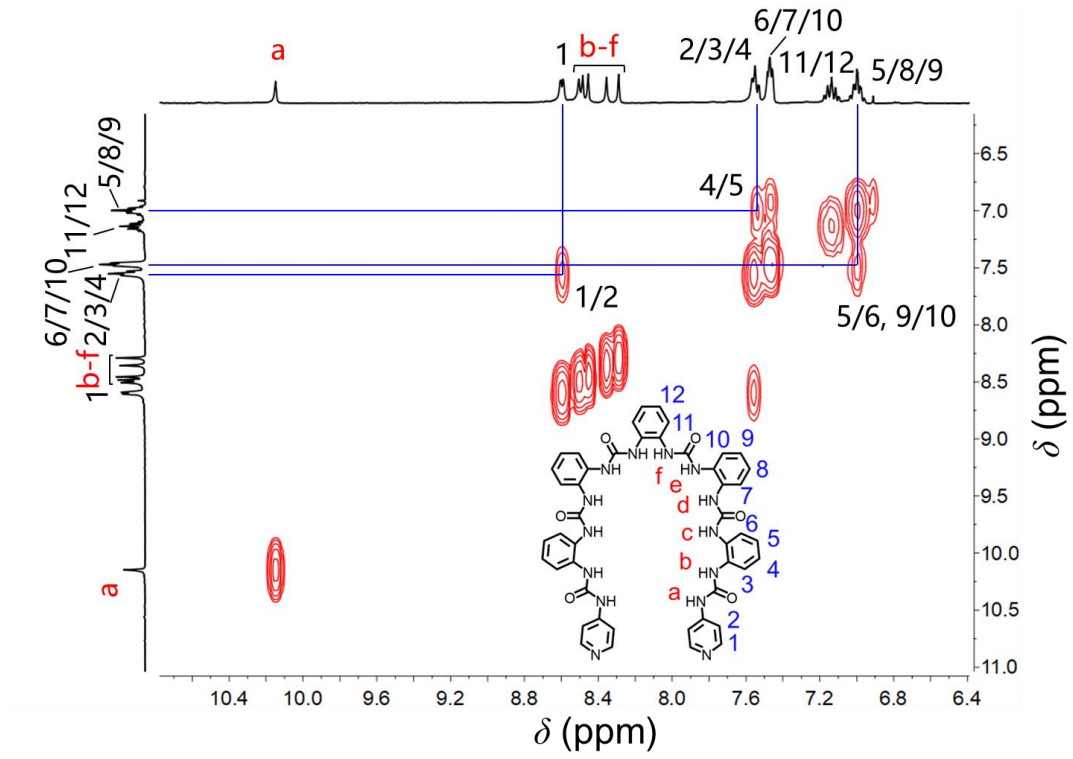

Figure S24. The ^{1}H-^{1}H COSY spectrum of $Pt_2\mathbf{L^1}_2(OTf)_4$ (2 mM, 400 MHz, DMSO-d_6, 298 K).

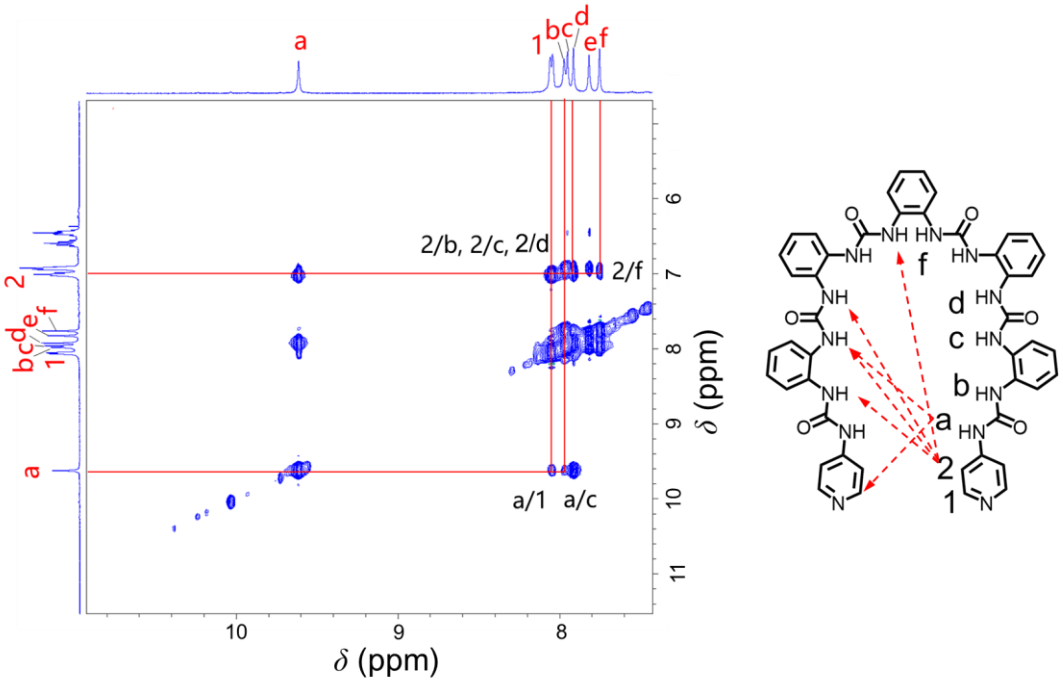

Figure S25. The ^{1}H-^{1}H NOESY spectrum of $Pt_2\mathbf{L^1}_2(OTf)_4$ (2 mM, 400 MHz, DMSO-d_6, 298 K).

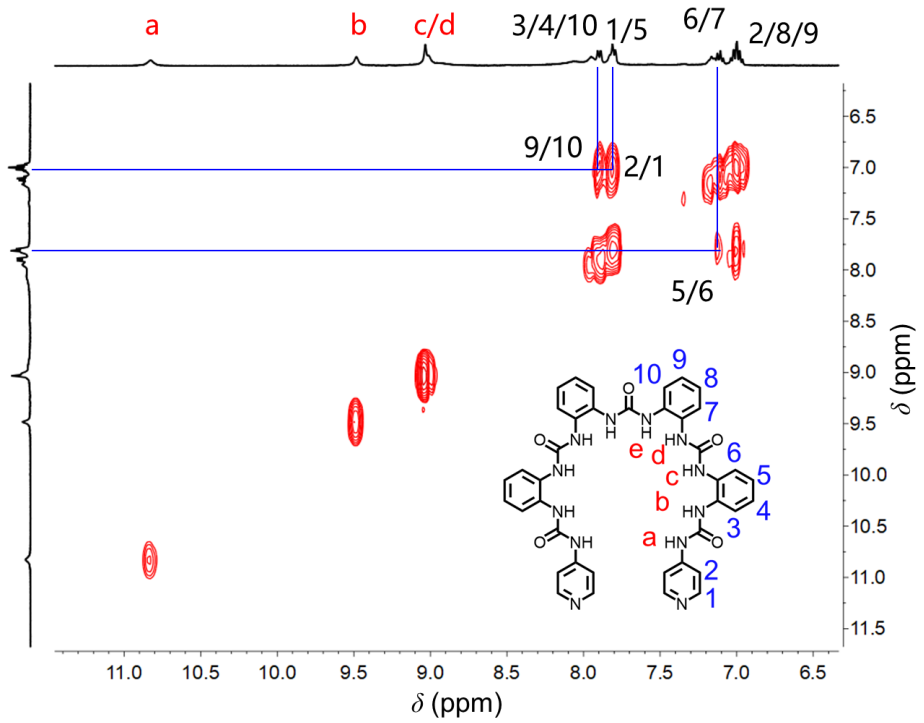

Figure S26. The ^{1}H-^{1}H COSY spectrum of $Pt_2\mathbf{L}^{2}_2(SO_4)_2$ (2 mM, 400 MHz, DMSO-d_6, 298 K).

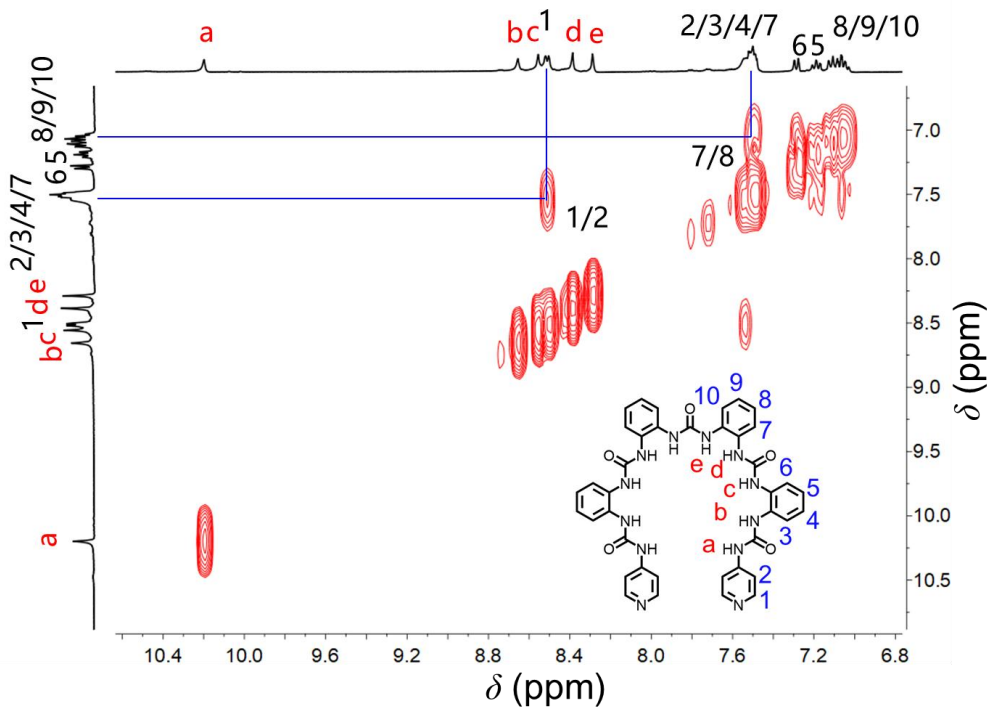

Figure S27. 2D ^{1}H-^{1}H NOESY spectrum of $Pt_2\mathbf{L}^{2}_2(OTf)_4$ (2 mM, 400 MHz, DMSO-d_6, 298 K).

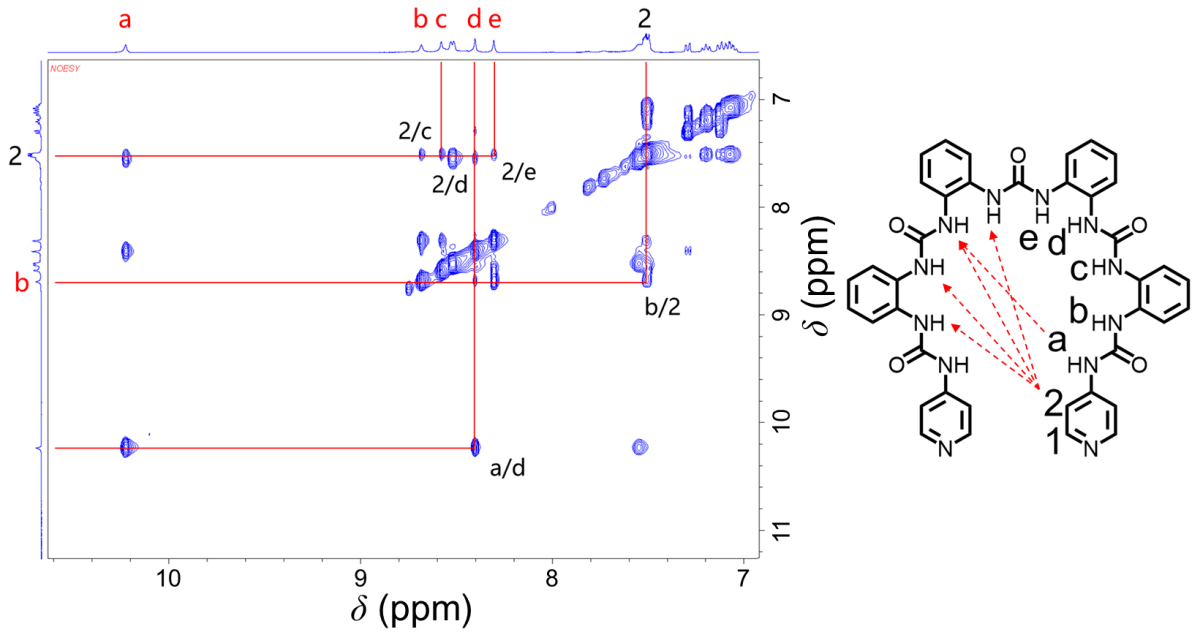

Figure S28 The ^{1}H-^{1}H NOESY spectrum of $Pt_2\mathbf{L}^{\mathbf{2}}_2(OTf)_4$ (2 mM, 400 MHz, DMSO-d_6, 298 K).

S7. Nucleotide Guest Recognition Results

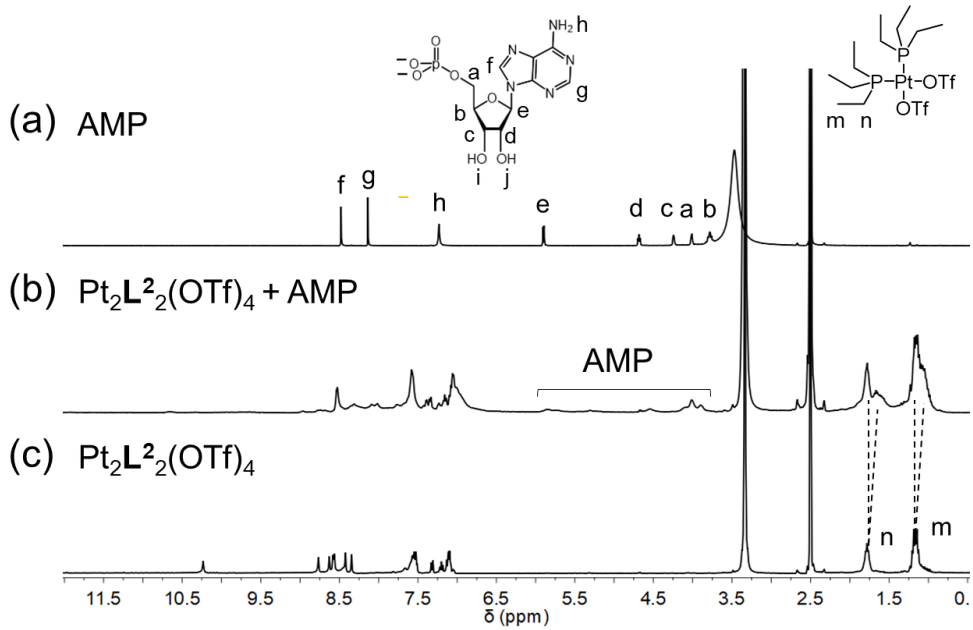

Figure S29. Stacked ^{1}H NMR spectra of (a) AMP, (b) $Pt_2\mathbf{L^2}_2(OTf)_4$ + AMP and (c) $Pt_2\mathbf{L^2}_2(OTf)_4$ (1 mM, 400 MHz, DMSO-d_6, 298 K). The broad NMR spectra for the aromatic region indicates the co-existence of multiple species, which could include the original $Pt_2L_2(OTf)_4$ complex and its binding with one- or two-AMP guest. In addition, the diastereomers of AMP ⊂ (+, +) $Pt_2\mathbf{L^1}_2$ and AMP ⊂ (-, -) $Pt_2\mathbf{L^1}_2$ complexes could also exist.

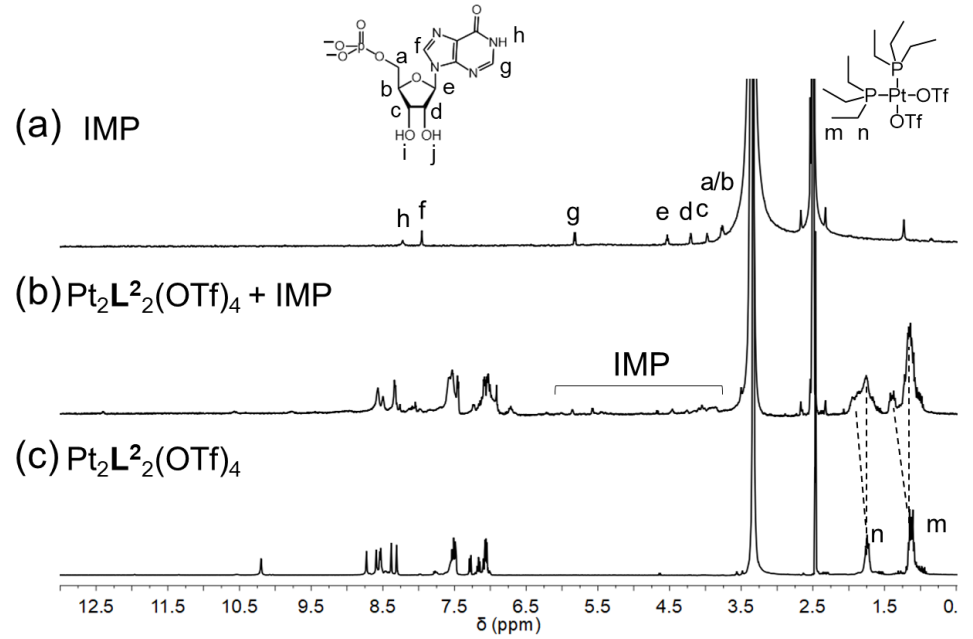

Figure S30. Stacked ^{1}H NMR spectra of (a) IMP, (b) $Pt_2\mathbf{L^2}_2(OTf)_4$ + IMP and (c) $Pt_2\mathbf{L^2}_2(OTf)_4$ (1 mM, 400 MHz, DMSO-d_6, 298 K).

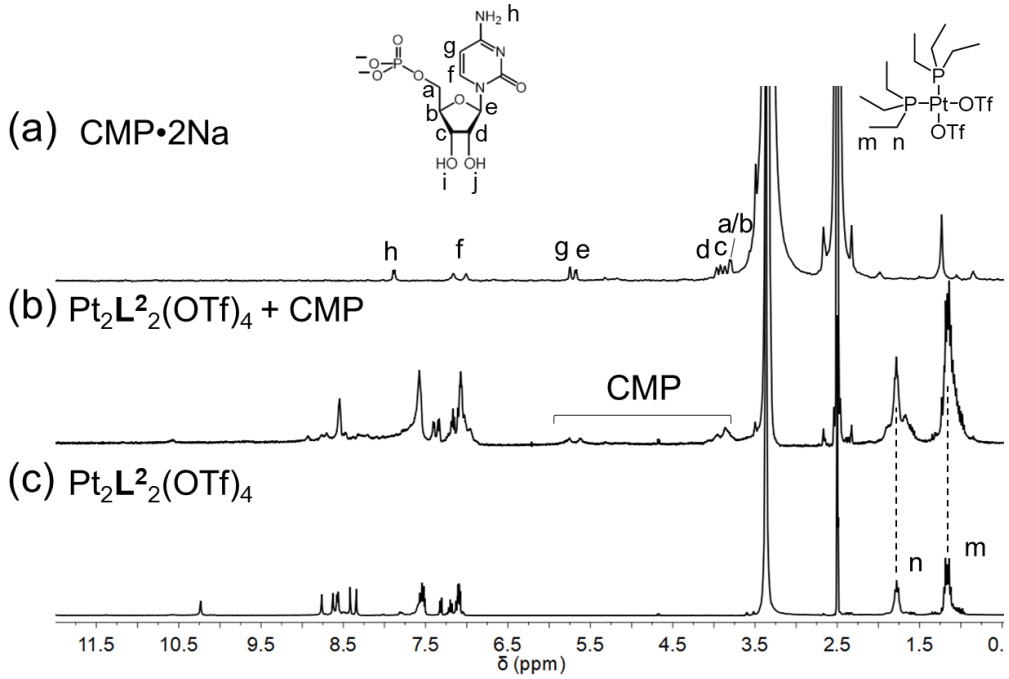

Figure S31. Stacked ^{1}H NMR spectra of (a) CMP, (b) $Pt_2\mathbf{L}^{\mathbf{2}}{}_2(OTf)_4$ + CMP and (c) $Pt_2\mathbf{L}^{\mathbf{2}}{}_2(OTf)_4$ (1 mM, 400 MHz, DMSO-d_6, 298 K).

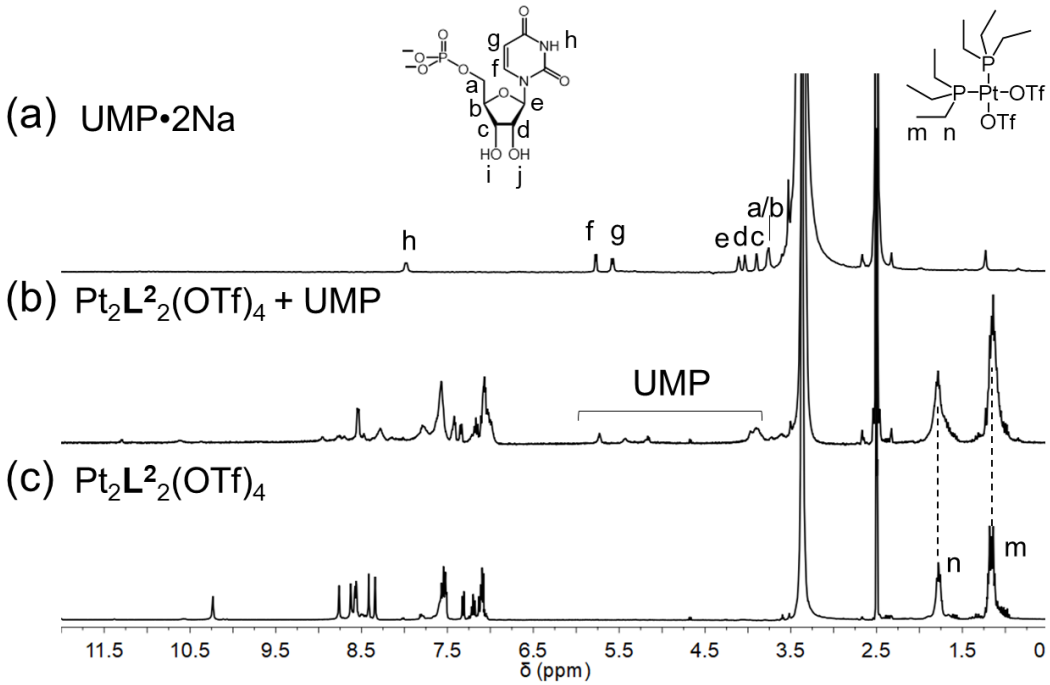

Figure S32. Stacked ^{1}H NMR spectra of (a) UMP, (b) $Pt_2\mathbf{L}^{\mathbf{2}}{}_2(OTf)_4$ + UMP and (c) $Pt_2\mathbf{L}^{\mathbf{2}}{}_2(OTf)_4$ (1 mM, 400 MHz, DMSO-d_6, 298 K).

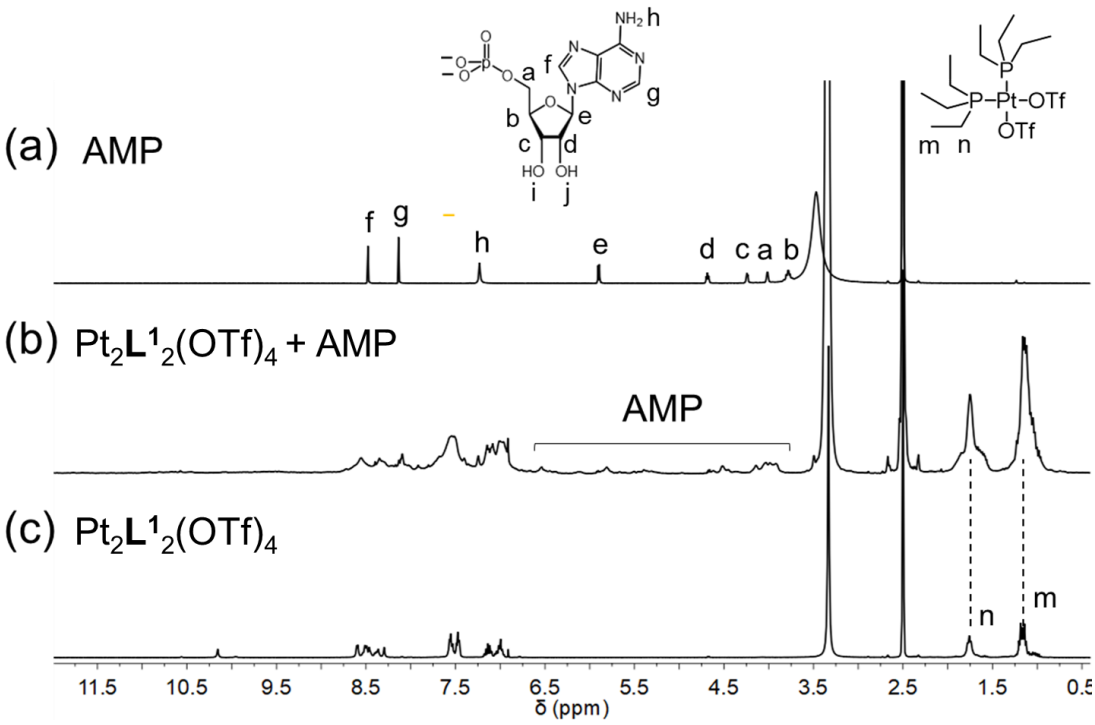

Figure S33. Stacked ^{1}H NMR spectra of (a) AMP, (b) $Pt_2\mathbf{L^1}_2(OTf)_4$ + AMP and (c) $Pt_2\mathbf{L^1}_2(OTf)_4$ (1 mM, 400 MHz, DMSO-d_6, 298 K).

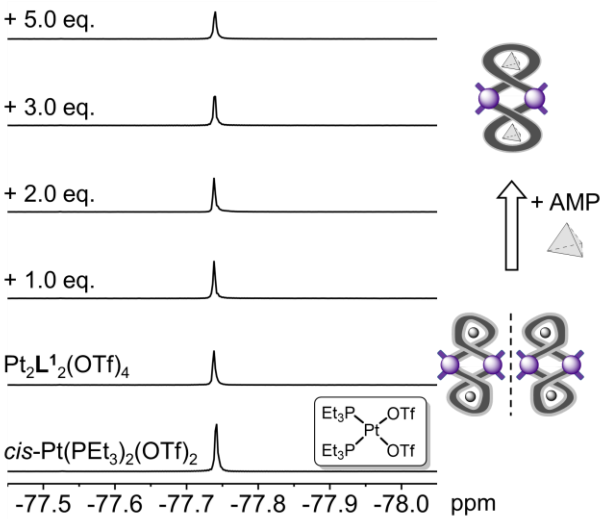

Figure S34. Stacked ^{19}F NMR spectra of the $Pt_2L_2(OTf)_4$ complex upon AMP binding (1 mM, 471 MHz, DMSO-d_6, CF_3COOH is used as external standard). The chemical shift changes of these complexes are negligible for the OTf binding and AMP anion exchange. This is likely attributed to the fact that OTf binding affinity with the oligourea backbone is too weak to induce noticeable ^{19}F NMR spectroscopic change.

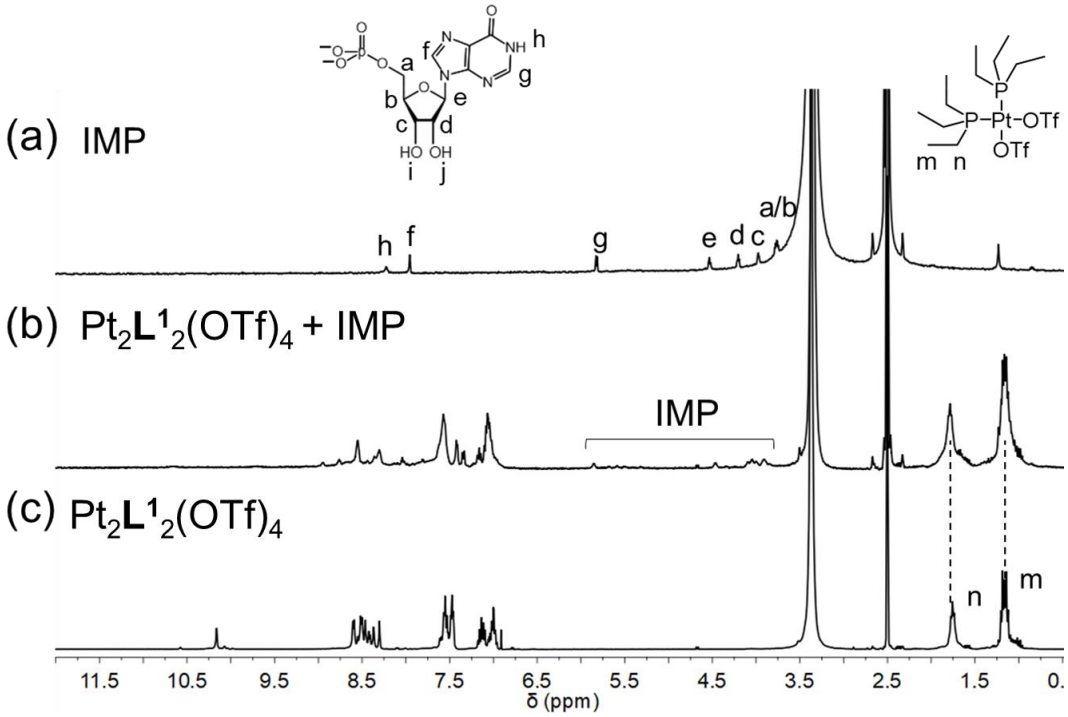

Figure S35. Stacked ^{1}H NMR spectra of (a) IMP, (b) $Pt_2\mathbf{L^1}_2(OTf)_4$ + IMP and (c) $Pt_2\mathbf{L^1}_2(OTf)_4$ (1 mM, 400 MHz, DMSO-*d*$_6$, 298 K).

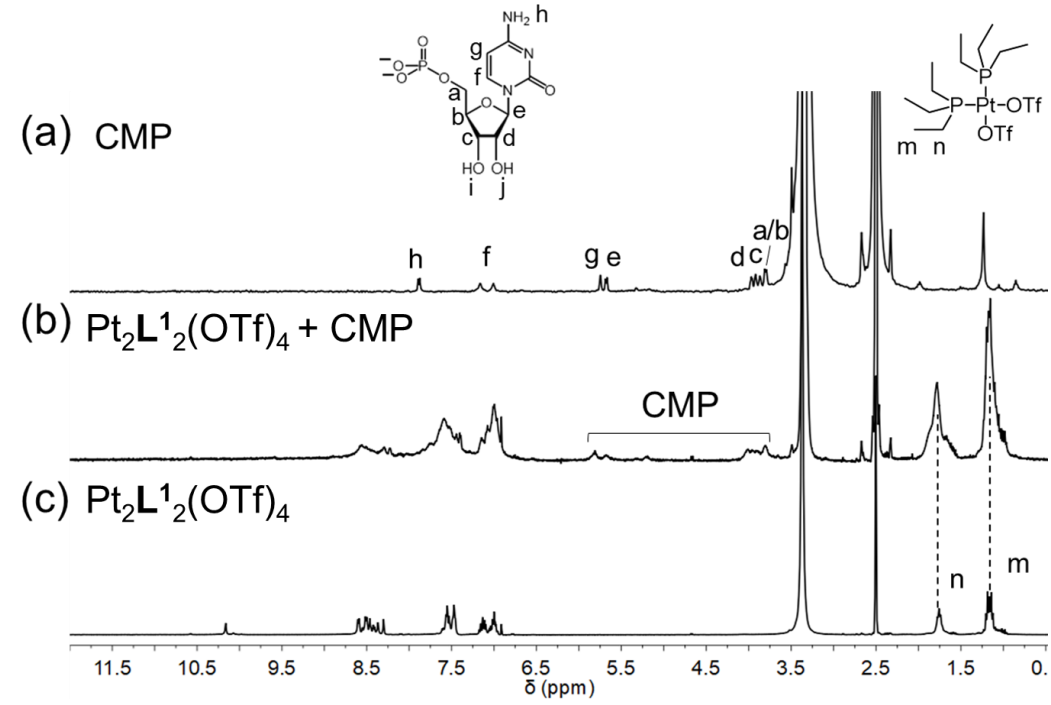

Figure S36. Stacked ^{1}H NMR spectra of (a) CMP, (b) $Pt_2\mathbf{L^1}_2(OTf)_4$ + CMP and (c) $Pt_2\mathbf{L^1}_2(OTf)_4$ (1 mM, 400 MHz, DMSO-*d*$_6$, 298 K).

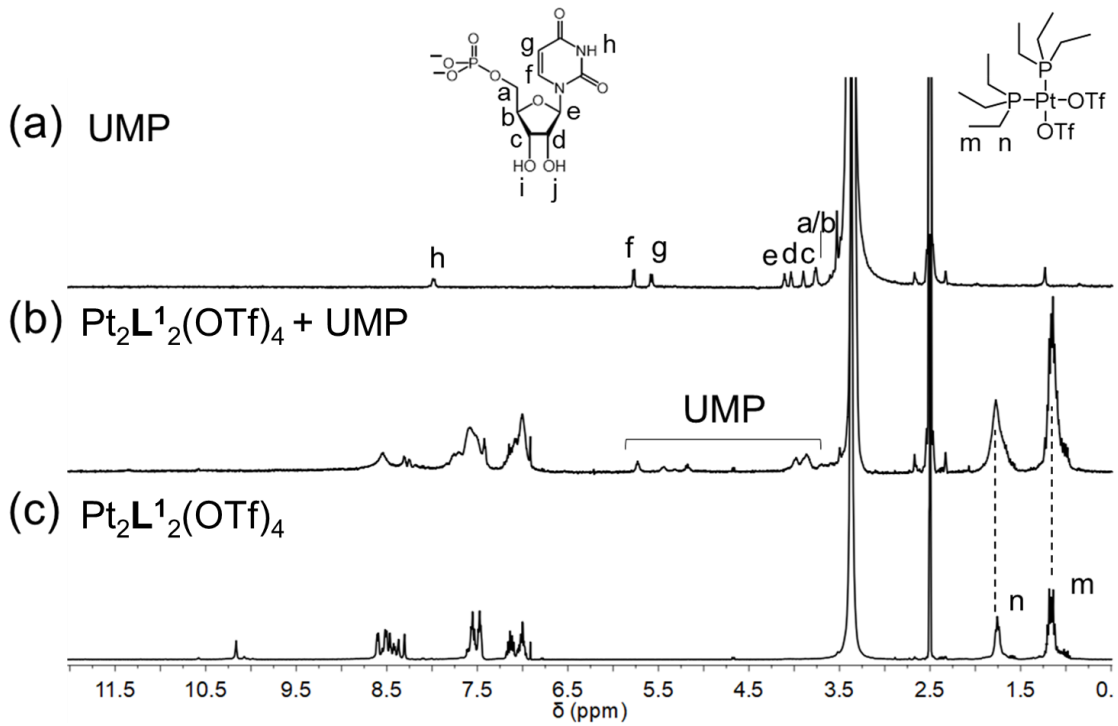

Figure S37. Stacked ^{1}H NMR spectras of (a) UMP, (b) $Pt_2\mathbf{L^1}_2(OTf)_4$ + UMP and (c) $Pt_2\mathbf{L^1}_2(OTf)_4$ (1 mM, 400 MHz, DMSO-d_6, 298 K).

To verify whether chiral induction or chiral recognition occurs upon AMP binding, we carefully compare these two processes (Figure S38, below). First, as supported by DFT calculations, the positively supercoiled AMP ⊂ (+, +) $Pt_2\mathbf{L^1}_2$ complex is more energy favored by 126 kJ/mol than that of the negatively supercoiled AMP ⊂ (-, -) $Pt_2\mathbf{L^1}_2$ complex. This suggests that AMP would bind to the (+, +) $Pt_2\mathbf{L^1}_2$ complex first thus inducing strong CD response. If the positive and negative supercoils are interconvertible, the AMP ⊂ (-, -) $Pt_2\mathbf{L^1}_2$ complex would change to the thermodynamically stable AMP ⊂ (+, +) $Pt_2\mathbf{L^1}_2$ complex, yielding continuous CD increase upon AMP binding (red curve in Figure x). In comparison, if the AMP-binding supercoils are not interconvertible, it is expected to see an increased CD intensity for the first formed AMP ⊂ (+, +) $Pt_2\mathbf{L^1}_2$ complex. As the amount of AMP is more than one equivalent (approximately 1.0 eq.), the AMP ⊂ (-, -) $Pt_2\mathbf{L^1}_2$ complex would form thus decreasing the CD single. Therefore, a stepwise CD change (increase-decrease) is believed to be seen upon AMP binding (blue curve, Figure S38). Experimentally, we only observed continuous CD increase upon AMP binding demonstrating the chiral induction process. Moreover, the oligourea backbone is highly flexible, and its binding with OTf anion is weak, which also supports interconvertible change of supercoils.

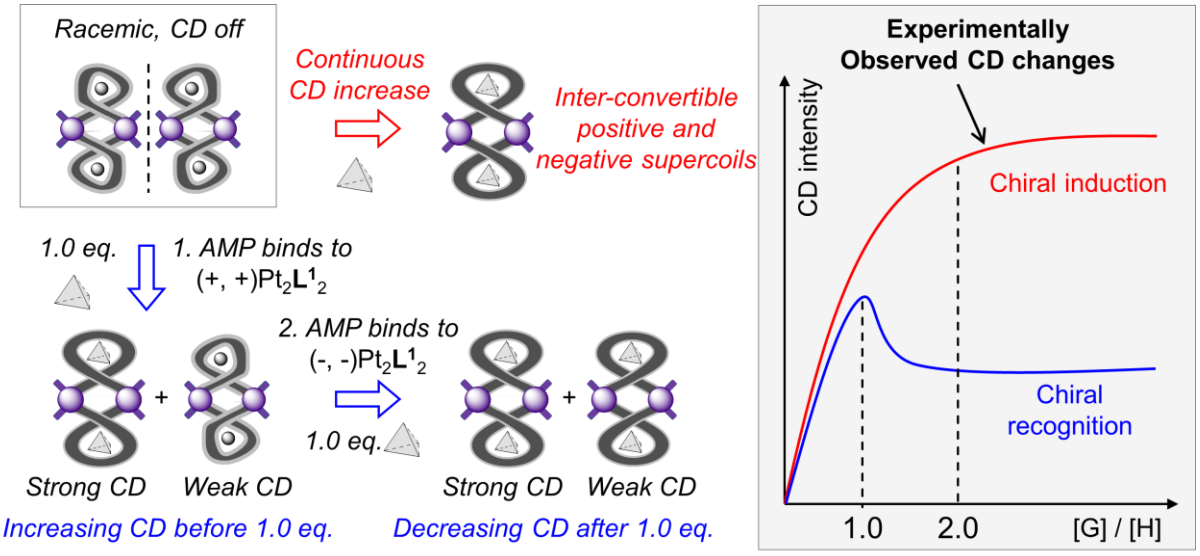

Figure S38. Schematic illustration for the comparison of AMP binding driven chiral induction (red curve) and chiral recognition (blue curve).

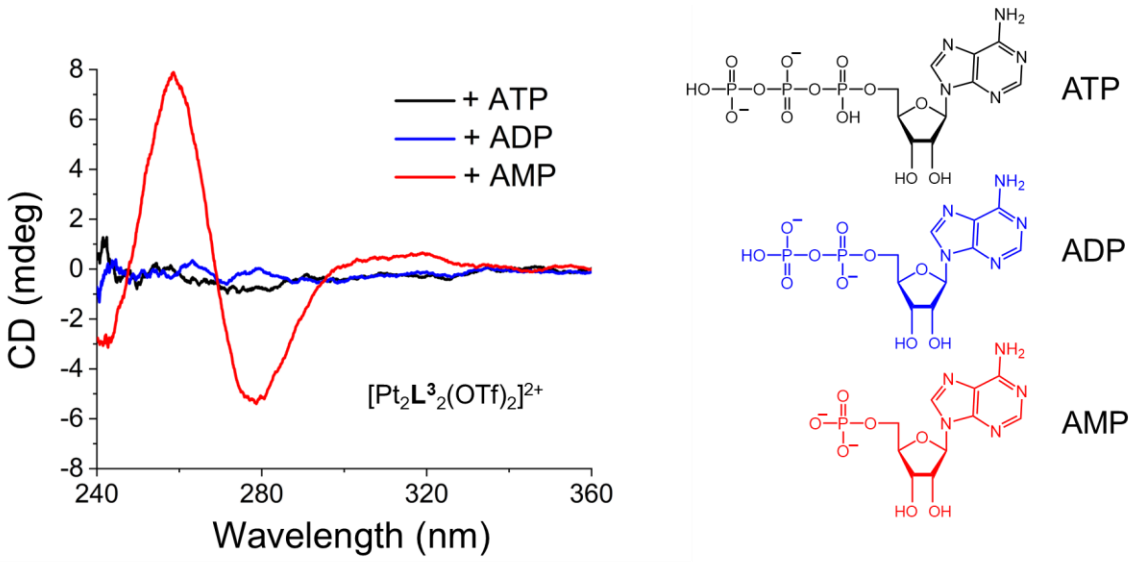

Figure S39. CD spectra of $Pt_2\mathbf{L^1}_2(OTf)_4$ (5×10^{-6} M) in the presence of two equivalents of AMP, ADP and ATP in 1% v/v DMSO/CH_3CN.

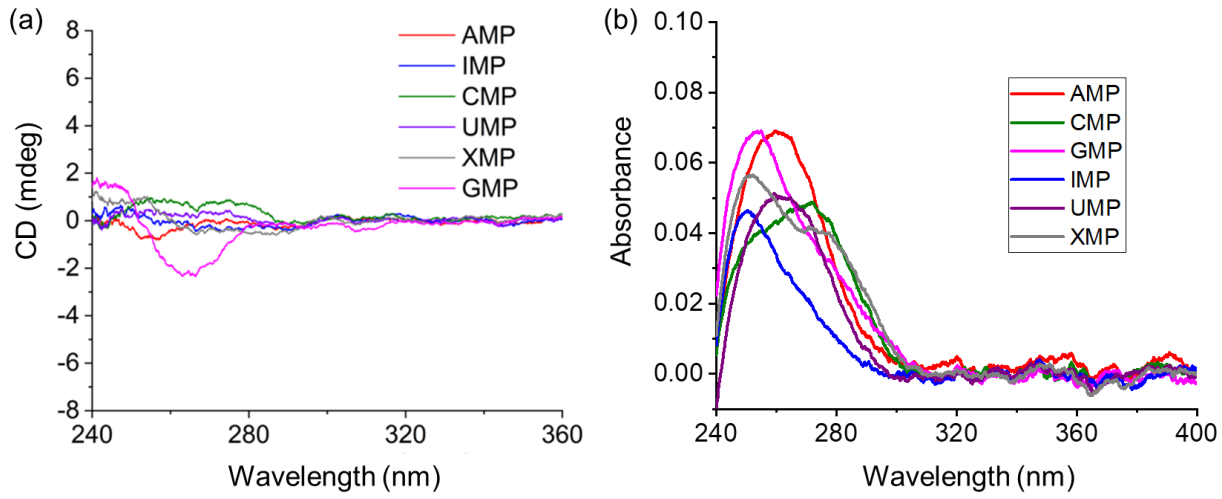

Figure S40. CD and UV-vis spectra of free nucleotides (50 µM) in 1% v/v DMSO/CH_3CN.

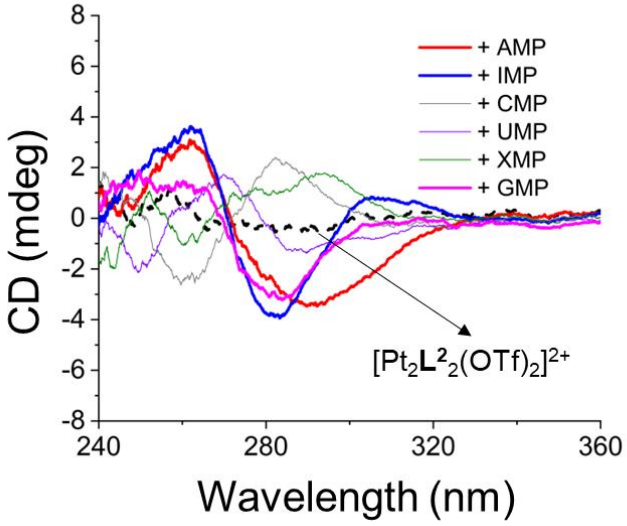

Figure S41. CD spectra (1% v/v DMSO/CH_3CN) of $Pt_2\mathbf{L^2}_2(OTf)_4$ (5×10^{-6} M) with two equivalents of various nucleotides.

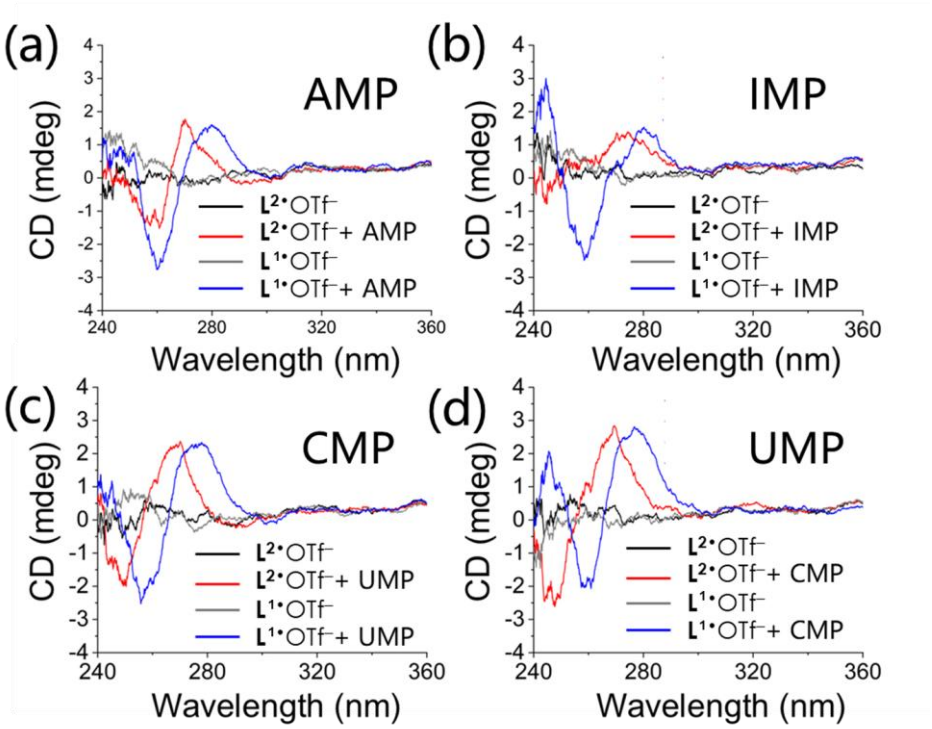

Figure S42. CD spectra (1% v/v DMSO/CH_3CN) of $Pt_2\mathbf{L^1}_2(OTf)_4$cand $Pt_2\mathbf{L^2}_2(OTf)_4$ complexes in presence of various nucleotides.

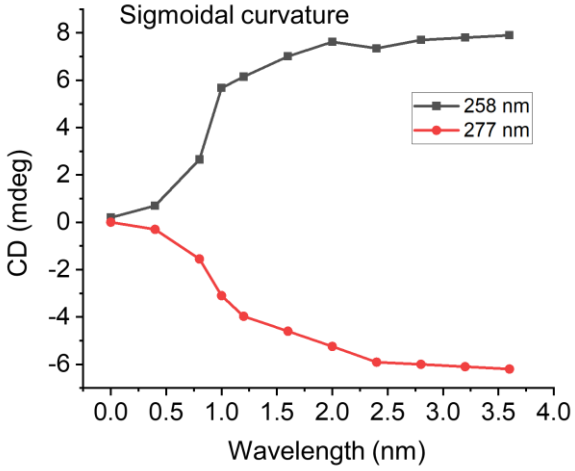

Figure S43. CD response of the $Pt_2L_2(OTf)_4$ complex (5 µM, 1% v/v DMSO/CH_3CN) upon AMP binding, which shows a sigmoidal curvature suggesting 1:2 binding stoichiometry and positive cooperativity for the AMP binding. We tried to estimate the AMP binding constant based on the CD titration data, unfortunately, no reliable result was determined according to the Bindfit fitting website. Notably, a clear sigmoidal curvature is displayed for the CD response of the $Pt_2L_2(OTf)_4$ complex upon AMP binding. This sigmoidal curvature is typically seen in enzyme-substrate

binding that indicates positive cooperativity and allosteric binding. Therefore, we think that positive cooperativity exists in the AMP binding with the supercoiling structures.

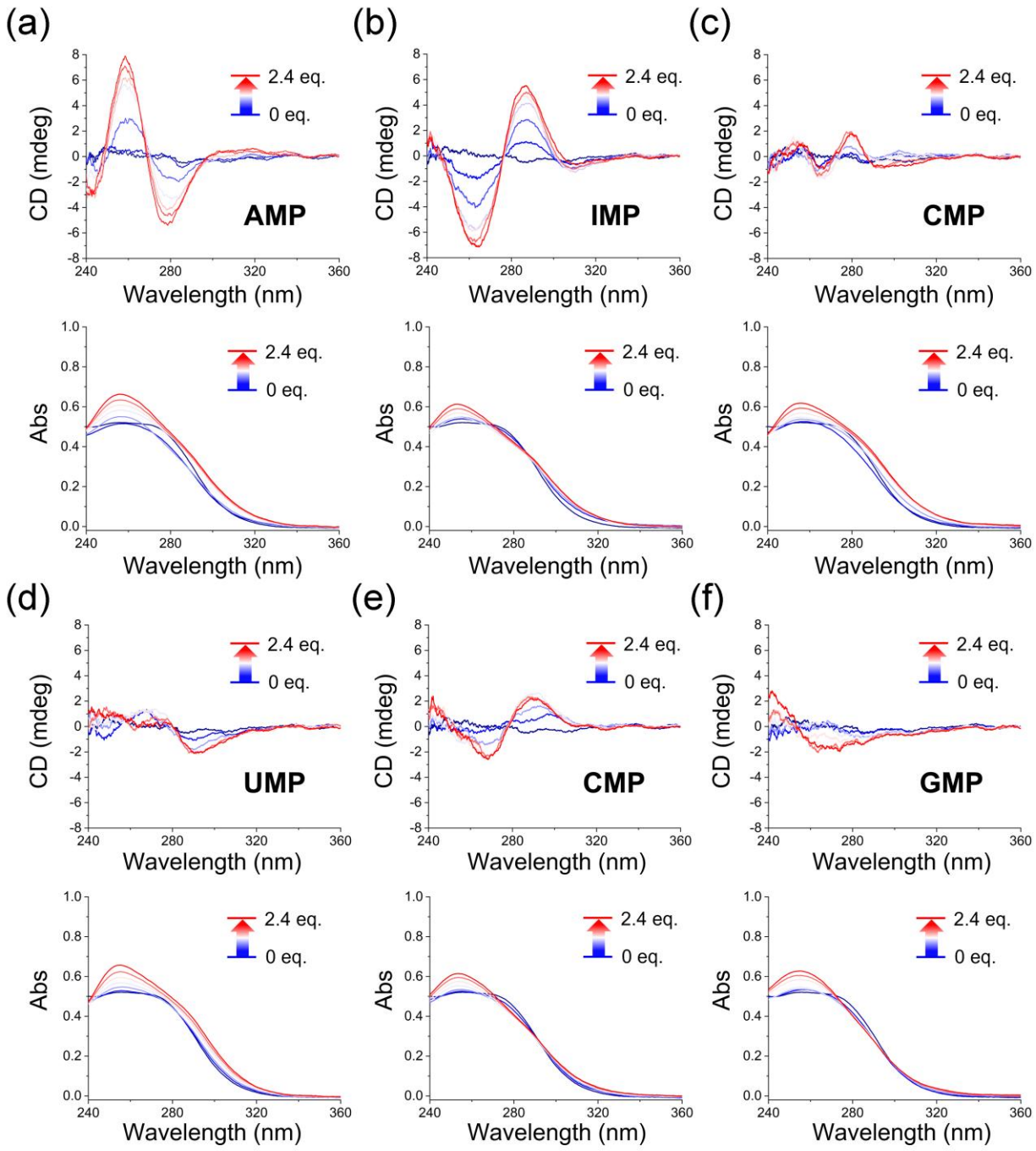

Figure S44. CD and UV-vis titration spectra of $Pt_2\mathbf{L^1}_2(OTf)_4$ (5×10^{-6} M) with (a) AMP, (b) IMP, (c) CMP, (d) UMP, (e) XMP and (f) GMP in 1% v/v DMSO/CH_3CN solution.

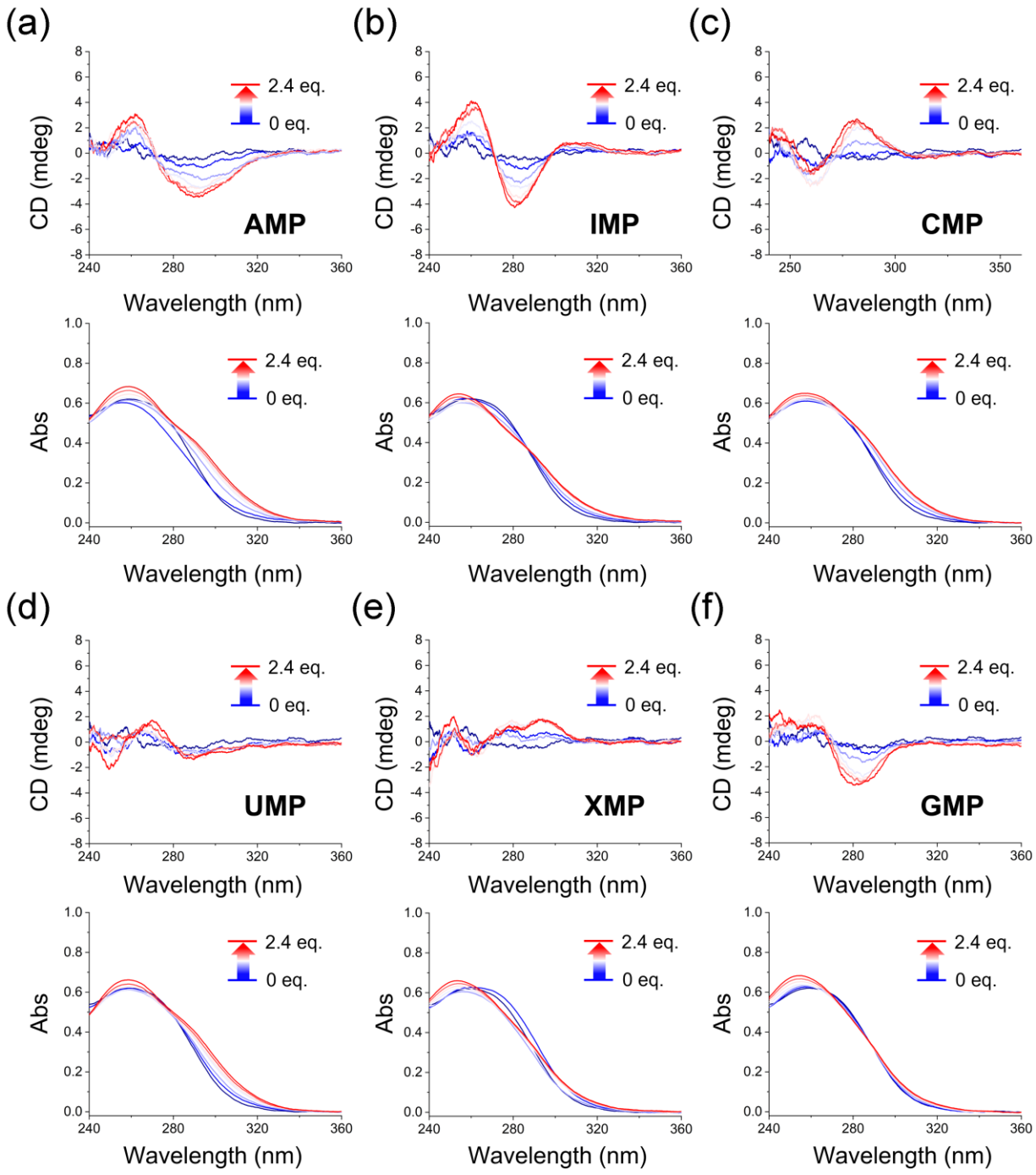

Figure S45. CD and UV-vis titration spectra of $Pt_2\mathbf{L}^2_2(OTf)_4$ (5×10^{-6} M) with (a) AMP, (b) IMP, (c) CMP, (d) UMP, (e) XMP and (f) GMP in 1% v/v DMSO/CH_3CN solution.

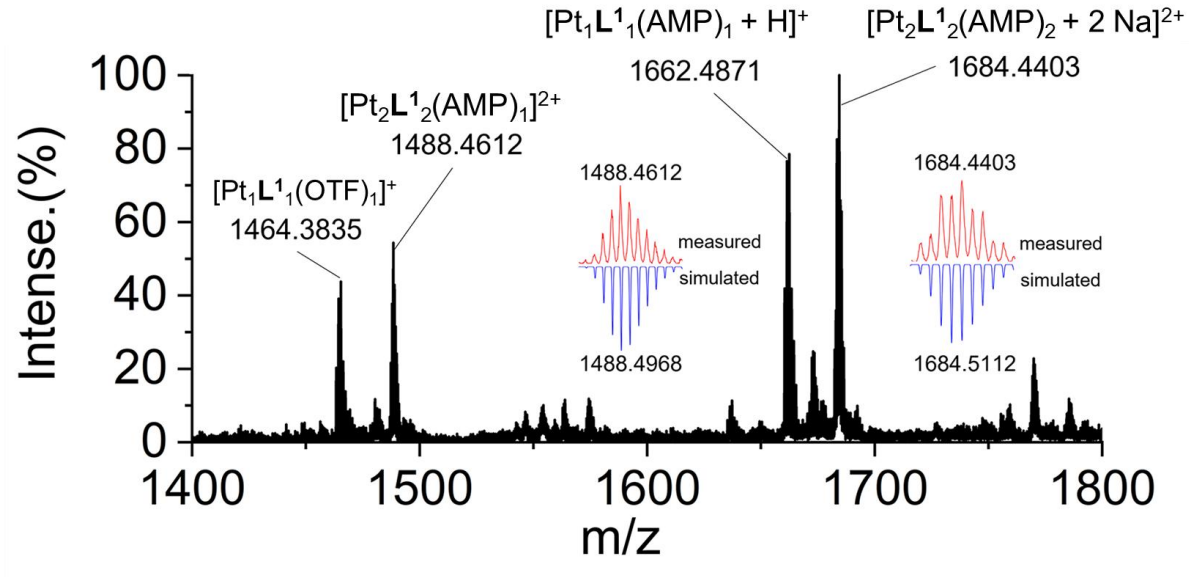

Figure S46. ESI-MS spectrum of $Pt_2\mathbf{L^1}_2(OTf)_4$ complex in the presence of AMP.

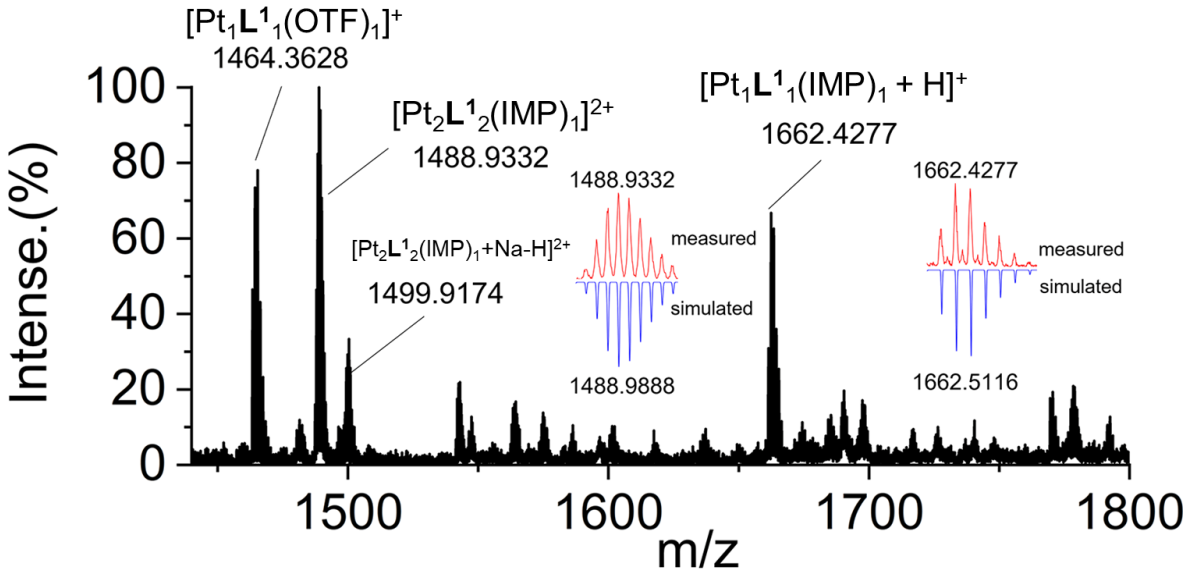

Figure S47. ESI-MS spectrum of $Pt_2\mathbf{L^1}_2(OTf)_4$ complex in the presence of IMP.

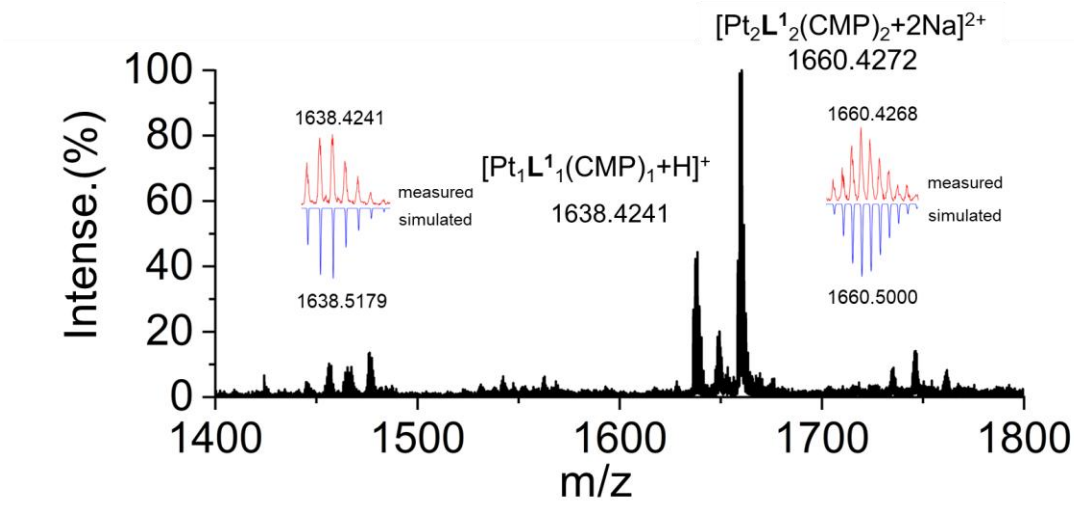

Figure S48. ESI-MS spectrum of $Pt_2\mathbf{L^1}_2(OTf)_4$ complex in the presence of CMP.

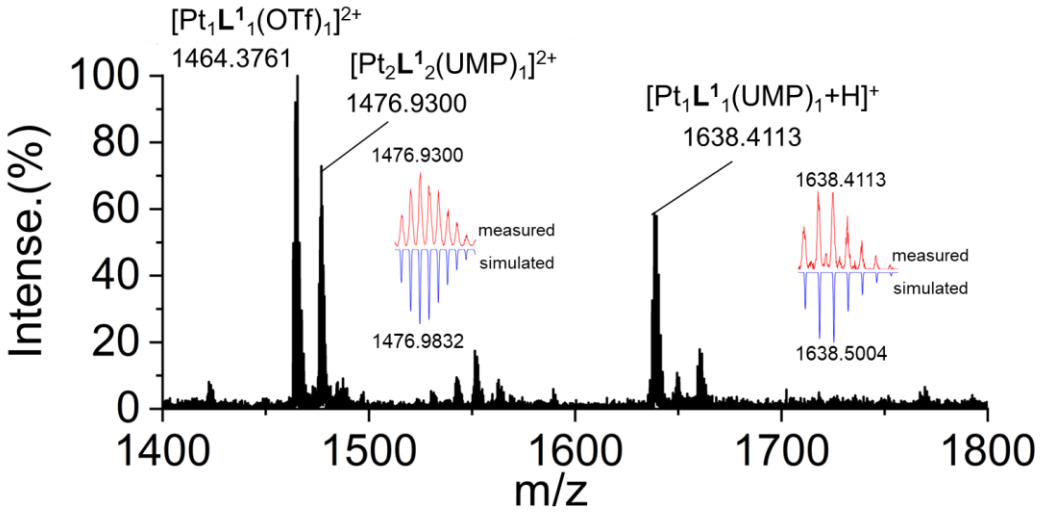

Figure S49. ESI-MS spectrum of $Pt_2\mathbf{L^1}_2(OTf)_4$ complex in the presence of UMP.

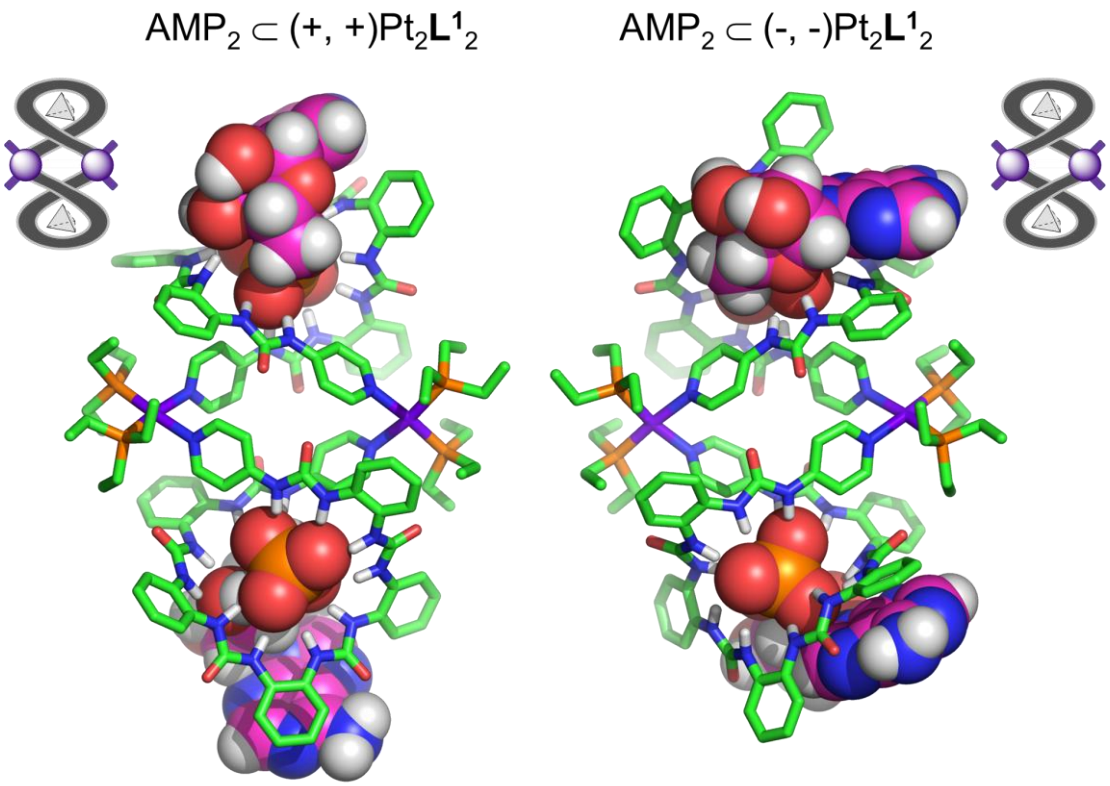

Figure S50. DFT-calculation optimized structure of (left) positively and (right) negatively supercoiled plectonemes upon AMP bindings. (M062X/6-31G*, implicit solvation, PCM model, in CH_3CN).

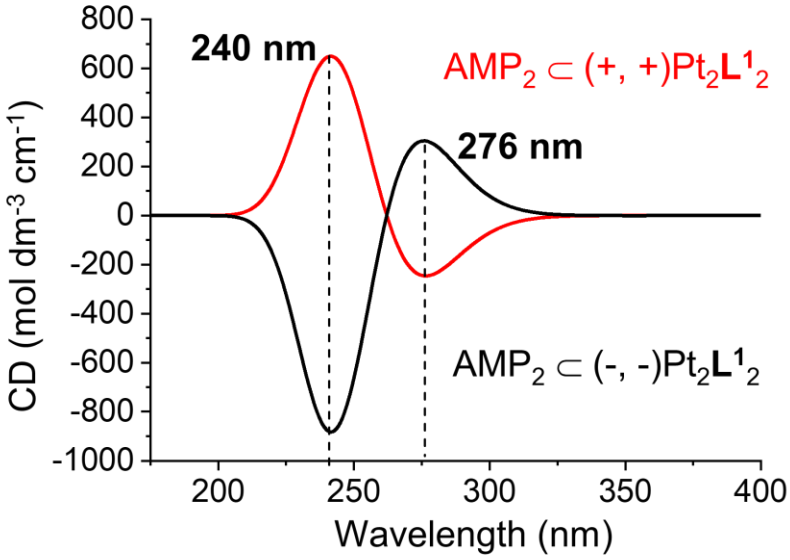

Figure S51. TD-DFT calculated CD spectra of positively and negatively supercoiled plectonemes upon AMP bindings. (M062X/6-31G*, implicit solvation: CH_3CN, PCM model).

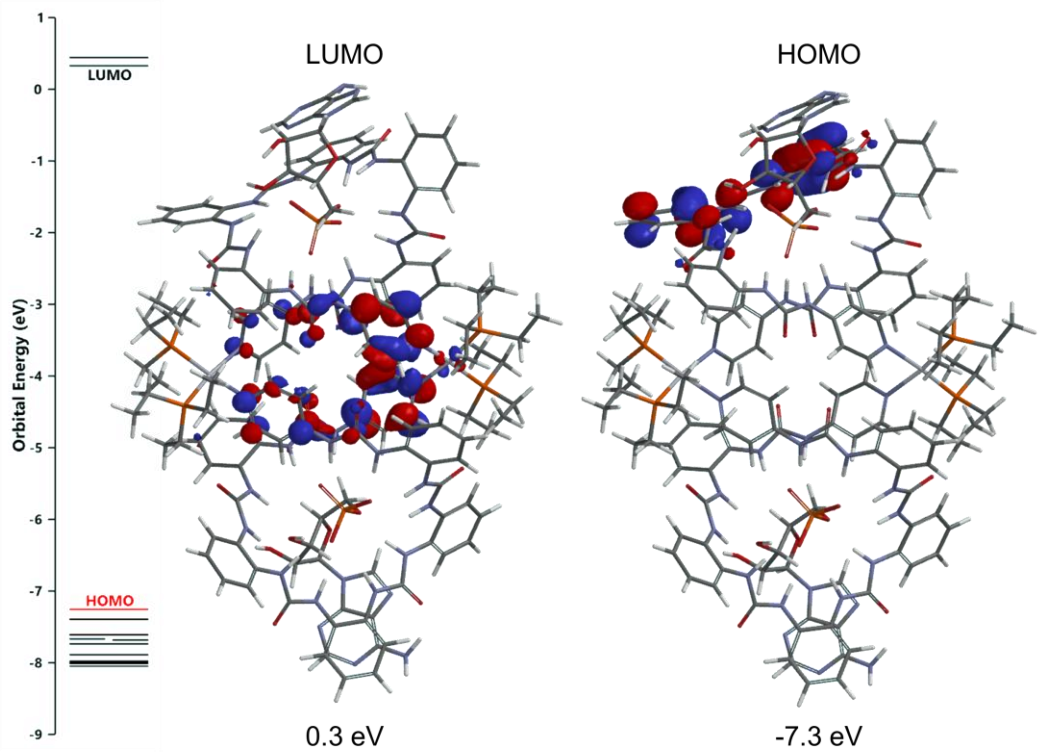

Figure S52. DFT calculated molecular orbitals for the AMP ⊂ (+, +) $Pt_2\mathbf{L^1}_2$ complex (M062X/6-31G*, implicit solvation: CH_3CN, PCM model).

S8. ^{1}H and ^{13}C NMR Spectra

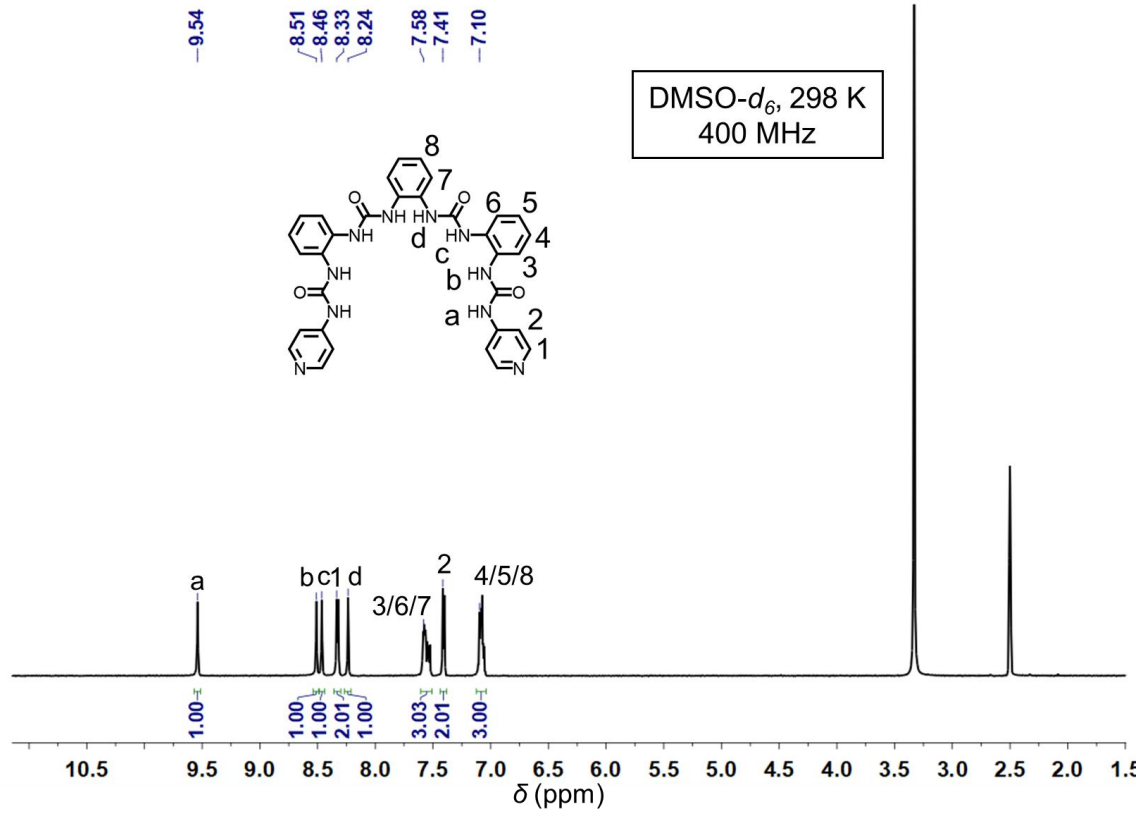

Figure S53. ^{1}H NMR spectrum (1 mM, 400 MHz, DMSO-d_6, 298 K) for ligand **L^{3}**.

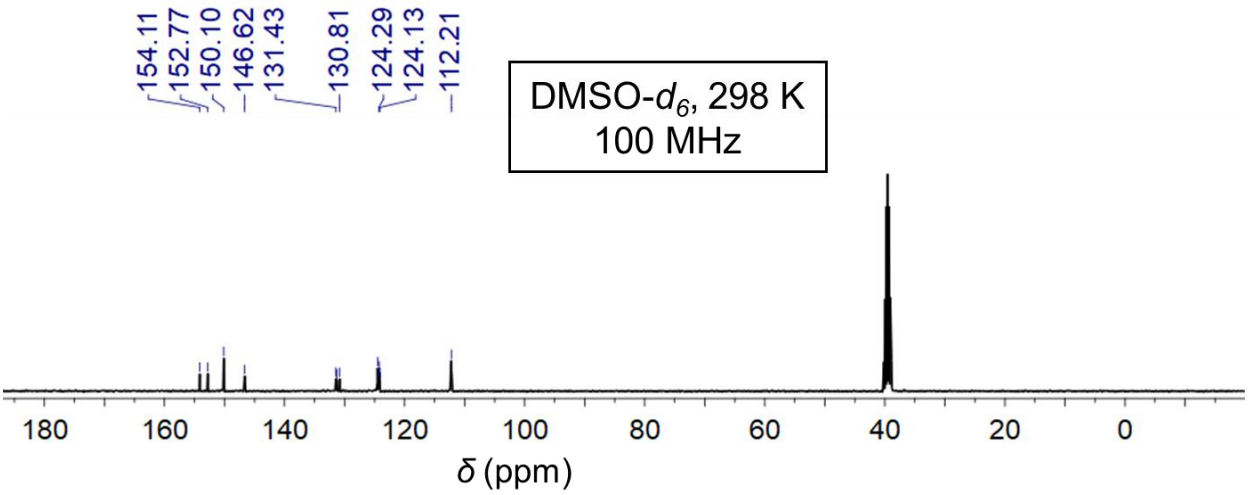

Figure S54. ^{13}C NMR spectrum (100 MHz, DMSO-d_6, 298 K) for ligand **L^{3}**.

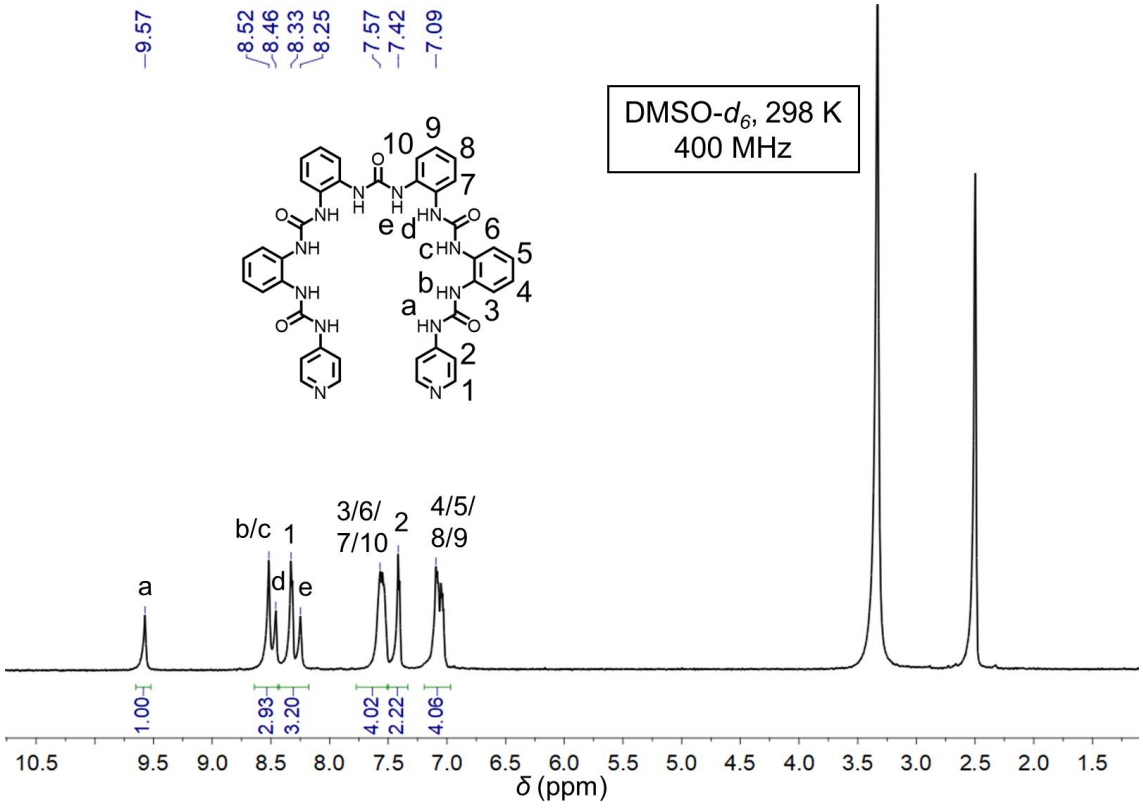

Figure S55. ^{1}H NMR spectrum (1 mM, 400 MHz, DMSO-d_6, 298 K) for ligand **L²**.

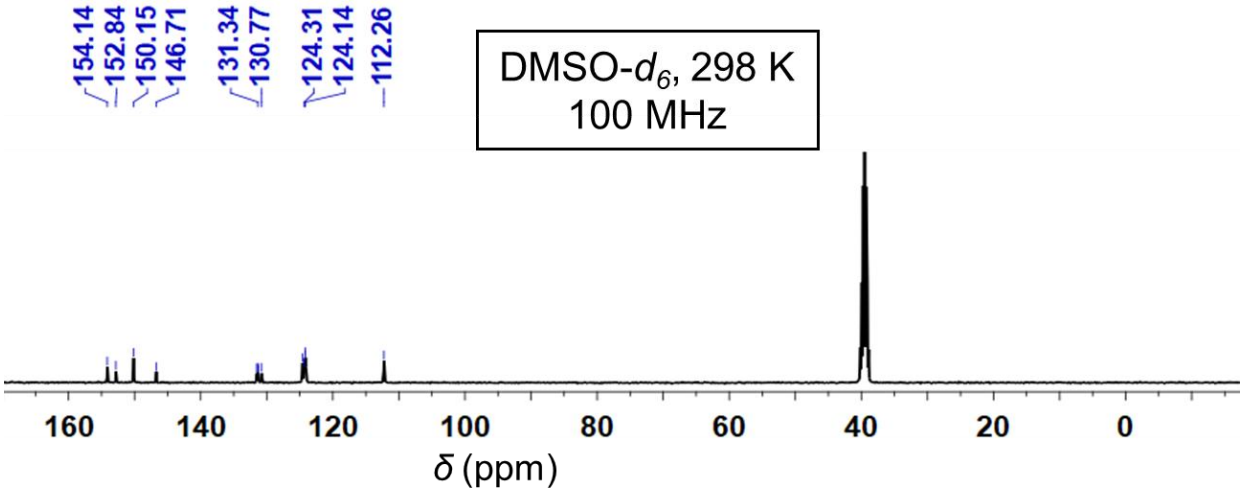

Figure S56. ^{13}C NMR spectrum (100 MHz, DMSO-d_6, 298 K) for ligand **L²**.

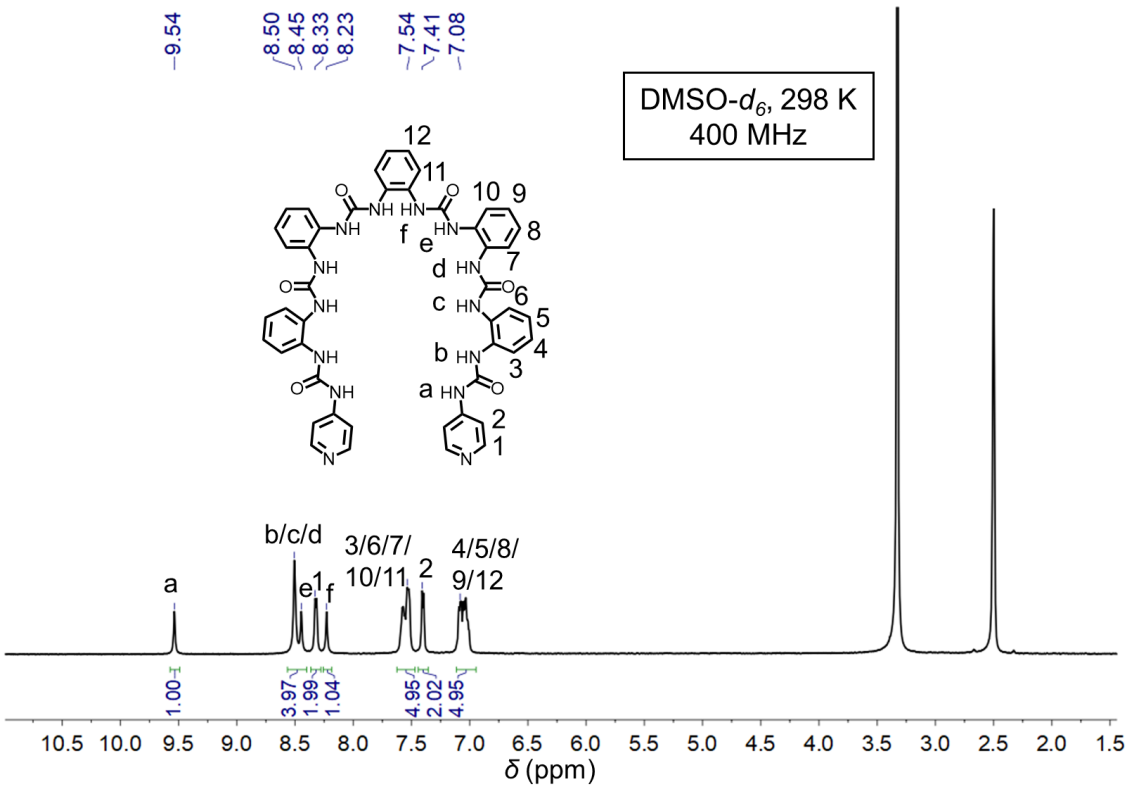

Figure S57. ^{1}H NMR spectrum (1 mM, 400 MHz, DMSO-d_6, 298 K) for ligand **L^{1}**.

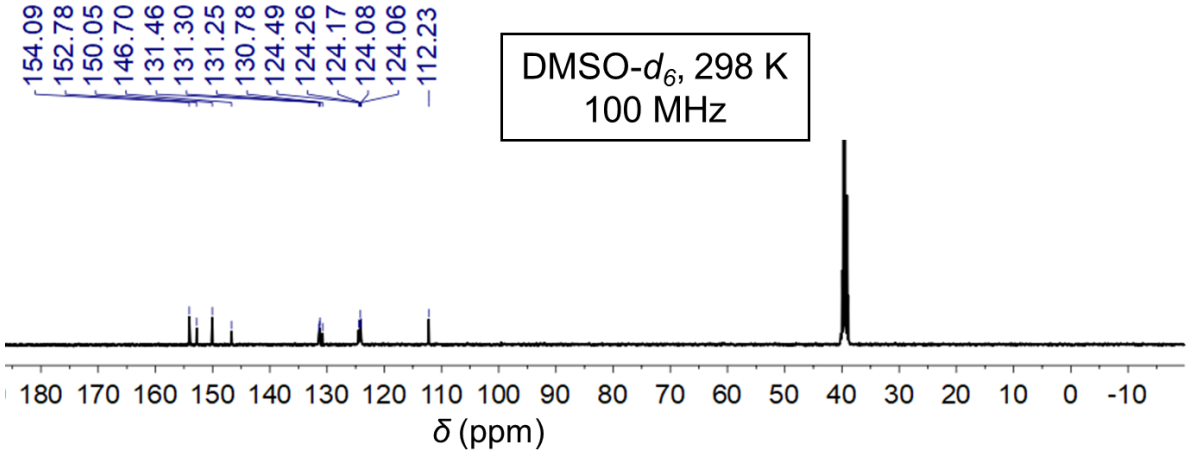

Figure S58. ^{13}C NMR spectrum (100 MHz, DMSO-d_6, 298 K) for ligand **L^{1}**.

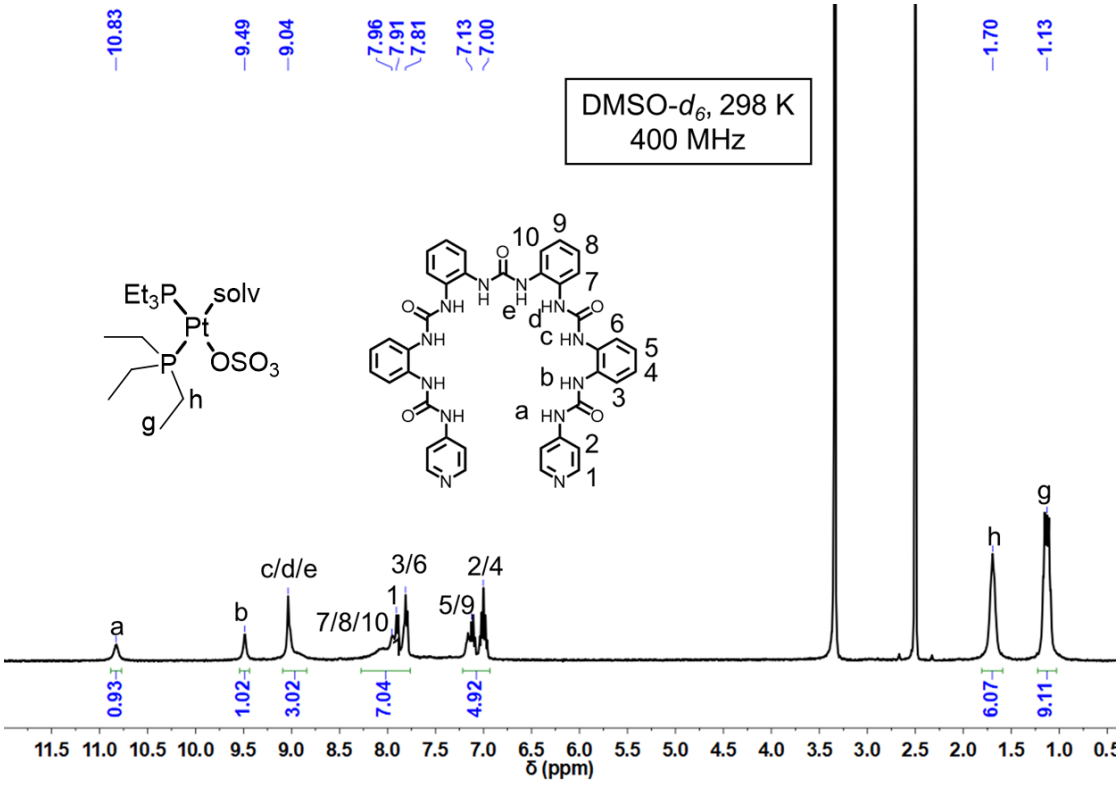

Figure S59. ^{1}H NMR spectrum (1 mM, 400 MHz, DMSO-d_6, 298 K) of $Pt_2\mathbf{L}^2{}_2(SO_4)_2$.

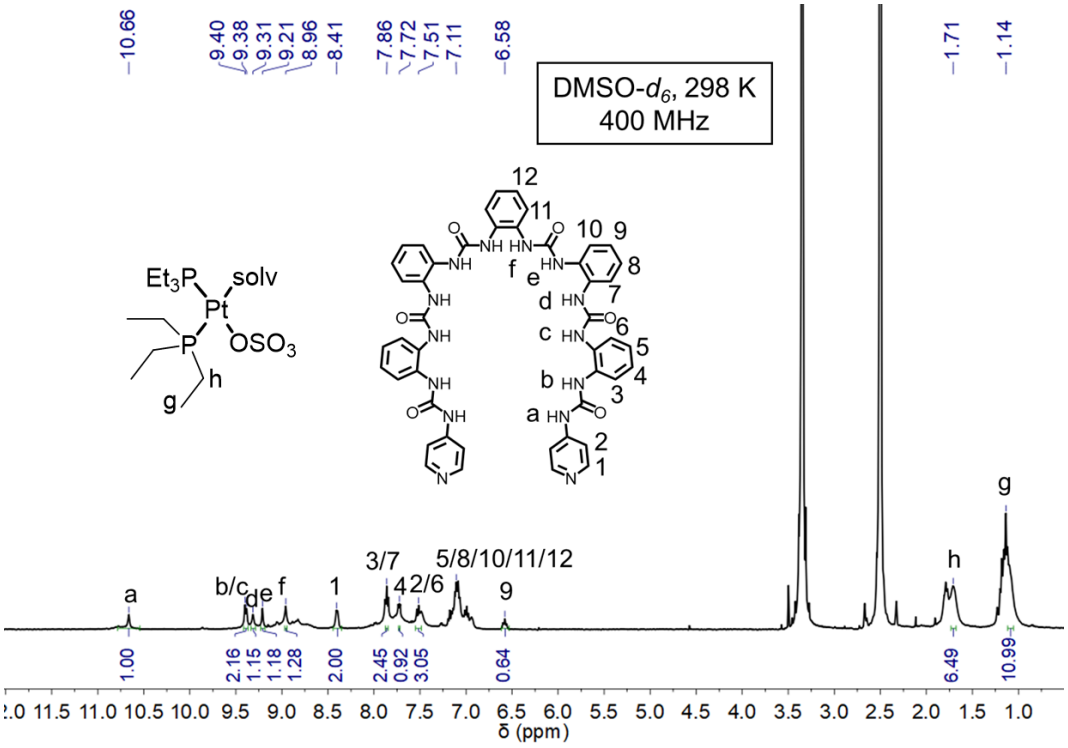

Figure S60. ^{1}H NMR spectrum (1 mM, 400 MHz, DMSO-d_6, 298 K) of $Pt_2\mathbf{L}^1{}_2(SO_4)_2$.

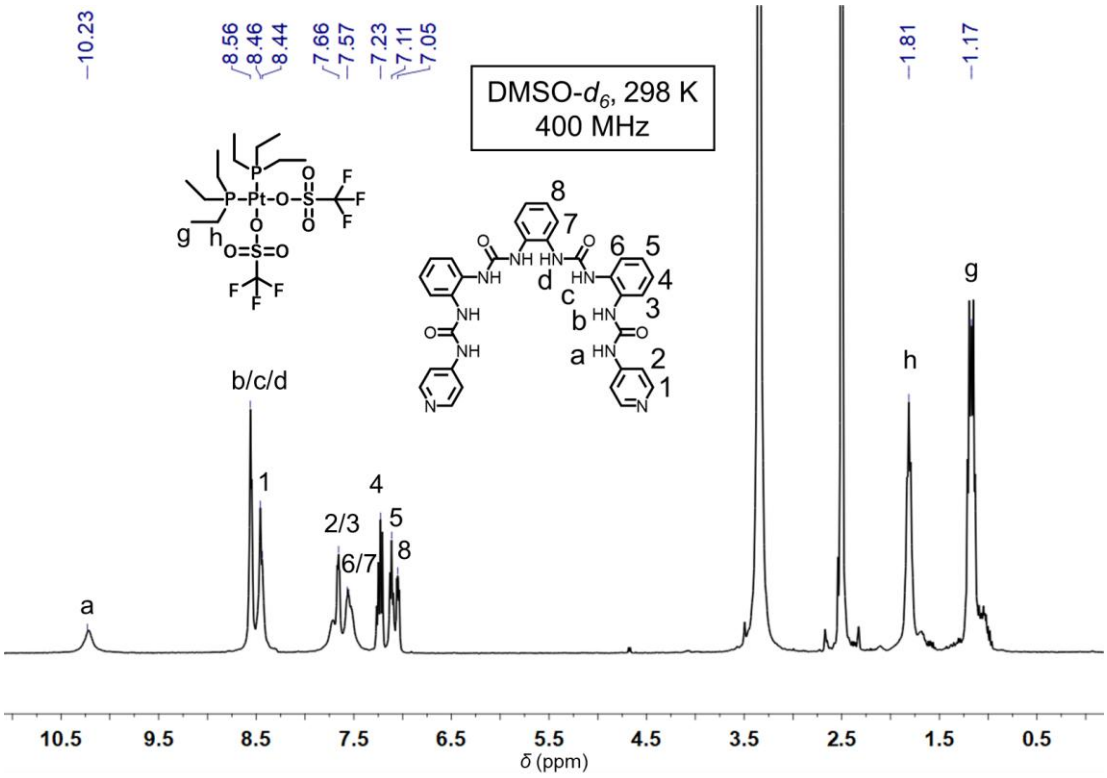

Figure S61. ^{1}H NMR spectrum (1 mM, 400 MHz, DMSO-d_6, 298 K) of $Pt_2\mathbf{L}^3{}_2(OTf)_4$.

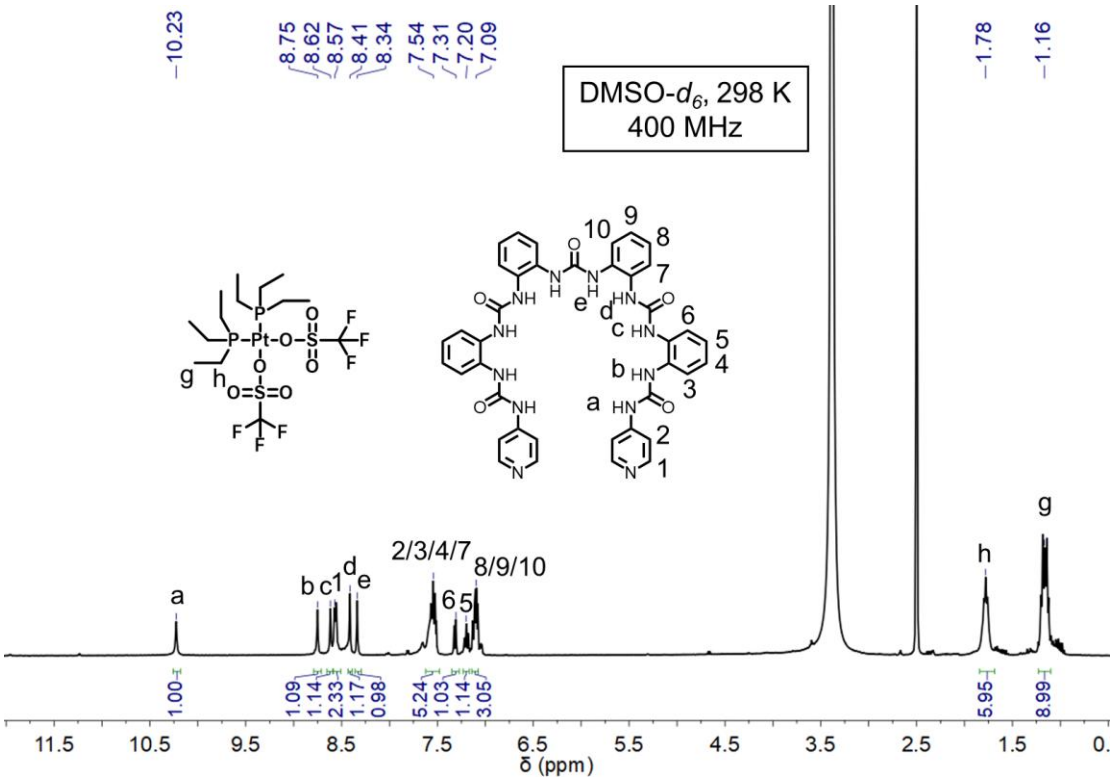

Figure S62. ^{1}H NMR spectrum (1 mM, 400 MHz, DMSO-d_6, 298 K) of $Pt_2\mathbf{L}^2{}_2(OTf)_4$.

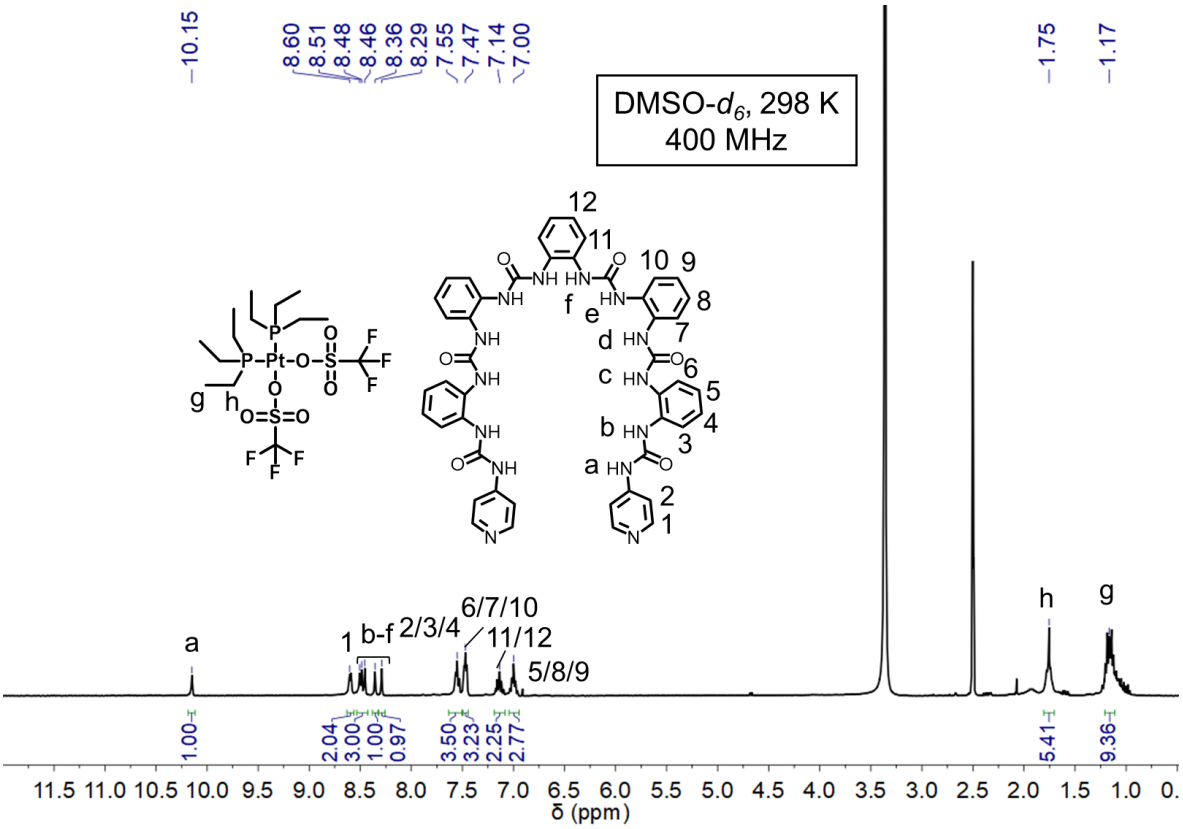

Figure S63. ^{1}H NMR spectrum (1 mM, 400 MHz, DMSO-d_6, 298 K) of $Pt_2\mathbf{L}^{\mathbf{1}}{}_2(OTf)_4$.

s